Thermalization in ultrarelativistic nuclear collisions. II. Entropy production and energy densities at the BNL Relativistic Heavy Ion Collider and the CERN Large Hadron Collider

Klaus Geiger
School of Physics and Astronomy, University of Minnesota, Minneapolis, Minnesota 55455
(Received 5 May 1992)

The dynamics of partons in ultrarelativistic ^{197}Au+^{197}Au collisions in the future collider experiments at the BNL Relativistic Heavy Ion Collider and the CERN Large Hadron Collider during the first 3 fm/c is simulated in full six-dimensional phase space within a parton cascade model to compute the entropy production and the space-time-dependent energy densities, temperatures, etc., in the central collision region. The partons' evolution from preequilibrium towards the formation of a thermalized quark-gluon plasma is investigated and compared to the Bjorken scenario. Moreover, an equation of state is extracted together with initial conditions for the further hydrodynamical space-time evolution of the matter. For central ^{197}Au+^{197}Au collisions with $\sqrt{s} = 200$–$6300A$ GeV the predictions for the energy densities and associated temperatures at $t = 3$ fm/c after the first instant of the collisions are ε =15–31 GeV/fm^3 and T =297–343 MeV, respectively. The multiplicity of final pions from the plasma is estimated from the amount of entropy produced, yielding a huge $dN^{(\pi)}/dy \simeq$1900–3400.

PACS number(s): 25.75.+r, 12.38.Bx, 12.38.Mh, 24.85.+p

I. INTRODUCTION

The production and observation of quark-gluon plasmas in ultrarelativistic heavy-ion collisions is one of the most ambitious goals of the experimental program of the Relativistic Heavy Ion Collider (RHIC) at Brookhaven and the Large Hadron Collider (LHC) at CERN. It is expected that very shortly (within a fraction of a fm/c) after the nuclei begin to overlap a large number of quarks and gluons are "freed" through frequent scatterings, eventually forming a hot, dense plasma of unconfined partons during the first few fm/c. Two of the most crucial questions in this context are the following: First, does the system reach a state of thermal (and chemical) equilibrium with sufficiently large volume and lifetime so that it may leave characteristic marks which survive the complex evolution from the deconfined quark-gluon phase to the hadronization yielding the final observed particles? Second, what are the signals that enable one to observe the formation of quark-gluon plasmas during the first 2–3 fm/c or so in the final particle spectra? Numerous theoretical papers addressing the properties and possible unambiguous signatures of this new form of matter have been published [1–3]. The most prominent proposed characteristic features are the spectra of photons [4–9] and dileptons [4,10–13] produced during the early stage of the collisions as well as the amount of strangeness [14–16] and charm [17–19] in the observed hadronic fragments. In studying the space-time evolution of a quark-gluon plasma, once it has been formed, it is usually assumed that relativistic hydrodynamics is applicable [20–26]. However, the validity of this convenient assumption remains to be checked. Futhermore, even if a hydrodynamical description is appropriate, one faces the problem of fixing the boundary and initial conditions as well as the equation of state. The major uncertainties are the initial conditions, since these depend on the poorly understood *preequilibrium* stage of the collision, that is, the space-time evolution of the collisions from the moment of nuclear overlap to the actual establishment of an equilibrated quark-gluon plasma.

The purpose of this paper is to examine these questions systematically within a realistic model, the parton cascade model presented in Refs. [27,28]. This model is based on the parton picture of hadronic interactions. It describes the preequilibrium dynamics of high-energy nuclear collisions in terms of the time evolution of the parton distributions in six-dimensional phase space by solving an appropriate transport equation in which the quark and gluon interactions are included within renormalization group improved perturbative QCD. A nuclear collision is described as a sequence of multiple hard and soft parton-parton scatterings and associated parton emission and absorption processes. In Ref. [28] I studied the microscopic characteristics of the space-time evolution of the partons during the preequilibrium stage of $A+A$ collisions with center-of-mass energy $\sqrt{s} = 200A$ GeV (A= mass number of the nuclei) and investigated the approach to an equilibrated quark-gluon plasma state in the central collision region. As a continuation, I will focus in the present paper on the macroscopic, thermodynamic properties of the parton system and discuss the observable implications. I will report on the results of simulations of central ^{197}Au+^{197}Au collisions with various beam energies from RHIC ($\sqrt{s} = 200A$ GeV) up to LHC ($\sqrt{s} = 6300A$ GeV). The time evolution of the energy, particle, and entropy densities is analyzed as the partons thermalize, from which the corresponding equation of state is extracted. In particular, I find for $\sqrt{s} = 200$–$6300A$ GeV, at $t = 3$ fm/c after the nuclei have touched, energy densities ε = 15–31 GeV fm^{-3}, particle densities n =17.5–28 fm^{-3}, specific entropies s/n =3.9–4.3, cor-

responding to temperatures of T =297–343 MeV. The extracted effective equation of state can be represented as $p(T) = a(T)T^4$, interrelating the pressure and the beam energy-dependent temperature $T = T(\sqrt{s})$. This equation of state includes the bulk of effects associated with parton interactions, finite quark masses, and a nonvanishing baryon-number density residing in the central collision region, important points which are generally neglected due to great complexity. To the best of my knowledge, this is the first attempt to rigorously extract realistic initial conditions for a hydrodynamical description of the further space-time evolution.

In this context the invariant total entropy produced during a nuclear collision plays an especially important role for several reasons.

(i) The entropy is a measure of equilibration. Its specific time development, as it approaches its asymptotic value during the nuclear collision, determines the equilibration time scale. It is an extensive quantity that is conserved throughout the subsequent hydrodynamical expansion [20].

(ii) In equilibrium the entropy density is simply related, via Gibb's law, to the energy density or particle density and the temperature of the system. Thus by calculating the local entropy density and the associated energy density, the corresponding temperatures can be extracted.

(iii) Most important for experimental detection, the entropy is a powerful tool for diagnosing quark-gluon matter. The amount of entropy produced can be independently determined by measuring the multiplicity of final pions $dN^{A+A\to\pi}/dy$, thereby providing a quantitative method for analyzing quark-gluon plasmas [20,21]. Furthermore, the amount of entropy produced is also reflected in the photon and dilepton emission rates from a plasma [10,11].

The outline of the paper is as follows. In Sec. II the general framework for calculating entropy, energy densities and number densities from the parton distributions is introduced. I will briefly review the widely employed Bjorken model [21] of the early space-time evolution in order to set the stage for a quantitative comparison with the results of the parton cascade model calculations. Also, it is pointed out how the total produced entropy is related to the observable multiplicity of pions. In Sec. III the actual details of the entropy computation with statistical methods are presented. It will be examined how the necessary discretization of phase space into cells affects the accuracy of the results and what the requirements for an appropriate cell configuration are. Section IV is devoted to the results of the model calculations for ^{197}Au+^{197}Au collisions over a range of beam energies $\sqrt{s}$ =200–6300 A GeV. The time evolution of the entropy, energy, and particle densities as the partons in the central region thermalize, as well as the beam energy dependence, will be shown. An effective equation of state plus initial conditions for a fluid dynamical expansion of the plasma will be extracted which are compared to the case of an ideal gas of noninteracting massless quarks and gluons—one of the approximations of the Bjorken picture. Finally, I will discuss the implications for the multiplicity of secondary hadrons (pions) produced from quark-gluon plasmas, which is observable in the experiments.

II. PARTON DYNAMICS AND ENTROPY PRODUCTION

A. Kinetic framework

In the kinetic framework of the parton cascade model [27,28] the time evolution of nuclear collisions is described by time-dependent single-particle distributions for the various parton species in the six-dimensional phase space: $F_a(r,p)$. Here $r \equiv r^\mu = (t,\mathbf{r})$ and $p \equiv p^\mu = (p^0,\mathbf{p})$ where $p^0 = E = \sqrt{\mathbf{p}^2 + m_a^2 + M^2}$ with m_a denoting the flavor-dependent quark rest mass and M a possible invariant virtual mass for partons that are off mass shell. The subscript a specifies the type of parton, $a = q_f, \bar{q}_f, g$ (quarks, antiquarks of flavor f, and gluons). The time evolution of the distribution functions is governed by a relativistic transport equation of the form ($\partial_\mu \equiv \partial/\partial r^\mu$):

$$p^\mu \partial_\mu F_a(r,p) = \sum_{\text{processes } k} I_a^{(k)}(r,p) \ . \tag{1}$$

The collision term on the right-hand side of the equation balances the various mechanisms by which partons may be gained or lost in an infinitesimal phase-space volume around $\mathbf{r}$ and $\mathbf{p}$ at time t through mutual interactions among the quanta. It is a sum of Lorentz-invariant collision integrals $I_a^{(k)}$ corresponding to the contributing interaction processes in which at least one parton of type a is involved.

The local space-time-dependent particle four-flow, entropy four-flow and energy-momentum tensor of the total system of partons are given by [29] ($\hbar = c = 1$)

$$\begin{aligned}
n^\mu(r) &= \sum_{a=g,q_f,\bar{q}_f} \gamma_a \int \frac{d^3p}{(2\pi)^3 p^0}\, p^\mu F_a(r,p), \\
s^\mu(r) &= -\gamma_g \int \frac{d^3p}{(2\pi)^3 p^0}\, p^\mu \Big\{ F_g(r,p)\ln[F_g(r,p)] - [1+F_g(r,p)]\ln[1+F_g(r,p)] \Big\} \\
&\quad - \sum_{a=q_f,\bar{q}_f} \gamma_a \int \frac{d^3p}{(2\pi)^3 p^0}\, p^\mu \Big\{ F_a(r,p)\ln[F_a(r,p)] + [1-F_a(r,p)]\ln[1-F_a(r,p)] \Big\}, \\
T^{\mu\nu}(r) &= \sum_{a=g,q_f,\bar{q}_f} \gamma_a \int \frac{d^3p}{(2\pi)^3 p^0} p^\mu p^\nu\, F_a(r,p).
\end{aligned} \tag{2}$$

The factors γ_a are the products of spin and color degeneracy, $\gamma_g = 2\times 8$ for gluons and $\gamma_q = \gamma_{\bar{q}} = 2\times 3$ for quarks and antiquarks. In the expression for s^μ, the first term is the gluon contribution, taking into account the Bose-Einstein statistics, whereas the second term is a sum over all quark and antiquark flavors with Fermi-Dirac statistics. From these equations the invariant scalars of number density, entropy density, and energy density, respectively, are obtained by contracting with the local flow velocity

$$u^\mu(r) \;=\; n^\mu(r)/\sqrt{n_\nu n^\nu} \quad , \tag{3}$$

so that

$$\begin{aligned} n(r) &= n_\mu(r)\; u^\mu(r), \\ s(r) &= s_\mu(r)\; u^\mu(r), \\ \varepsilon(r) &= T_{\mu\nu}(r)\; u^\mu(r) u^\nu(r). \end{aligned} \tag{4}$$

These quantities can be measured in the local rest frame of the matter where $u^\mu = (1,\mathbf{0})$. The total number, entropy, and energy of particles at a given time can therefrom be obtained by integrating over coordinate space. As will be explained in Sec. III, the practical computation of these densities within the parton cascade model proceeds by dividing phase space in cells and estimating the parton distributions by counting the number of partons in each cell, from which the densities are computed in the local rest frame of the individual cells.

Relativistic kinetic theory [29] states that if the distribution functions F_a of the particles tend to a definite limit as time progresses, the system develops into an equilibrium state. In this steady state the entropy of the system attains its maximum value. Therefore a necessary condition for equilibrium is that the entropy production vanishes in space-time. This condition together with the requirement that the distribution functions must be a solution of the transport equation (1) uniquely determines their form:

$$F_a^\pm(r,p) = \frac{1}{\exp\left[\beta_\nu(p^\nu - \lambda_a^\nu)\right] \pm 1} \quad . \tag{5}$$

Here p_ν is the four-momentum of the particle and the upper sign refers to fermions (quarks) and the lower sign to bosons (gluons). $\lambda_\nu(r)$ and $\beta_\nu(r)$ are space-time dependent four-vectors constructed from the local flow velocity $u_\nu(r)$, the local chemical potentials $\mu_a(r)$ (one for each quark species) and the inverse local temperature $\beta(r) = 1/T(r)$:

$$\begin{aligned} \lambda_a^\nu(r) &= \mu_a(r) u^\nu(r), \\ \beta^\nu(r) &= \beta(r) u^\nu(r) \quad . \end{aligned} \tag{6}$$

Whereas the gluon chemical potential necessarily is zero [28,16], the quark chemical potentials μ_a measure the number of quarks minus antiquarks, i.e., the baryon density and electric charge.

Once the system of partons has reached an equilibrium state, its further evolution can be described within the framework of relativistic hydrodynamics according to the hydrodynamic equations:

$$\begin{aligned} \partial_\mu T^{\mu\nu}(r) &= 0, \\ \partial_\mu n^\mu(r) &= 0 \quad . \end{aligned} \tag{7}$$

Whereas the first equation is a consequence of energy-momentum conservation, the second equation follows from (1) by integrating over d^3p and the fact that the collision term vanishes, if the system is in a thermal and chemical equilibrium state with the distribution functions taking the form (5). In the absence of dissipation the energy-momentum tensor can be written in terms of the proper energy density $\varepsilon(r)$, the pressure $p(r)$ and the local flow velocity $u^\mu(r)$, Eq. (3):

$$T^{\mu\nu}(r) \;=\; -g^{\mu\nu}\, p(r) \;+\; \Big(\,\varepsilon(r) \;+\; p(r)\Big)\; u^\mu(r) u^\nu(r) \,. \tag{8}$$

The details of the space-time development of the system will depend on its equation of state $\varepsilon(p)$, or equivalently, $p(T)$, interrelating the local energy density ε, pressure p, and temperature T. For an ideal quark-gluon plasma consisting of massless partons with chemical potentials μ_a for the (anti)quarks and the inclusion of parton interactions up to order g^3T^4 within perturbative QCD the equation of state may be derived from the thermodynamic potential [30,31]

$$\Omega(T,V,\mu_a) \;=\; -\,V\; a(T,\mu_a,g)\; T^4 \quad , \tag{9}$$

where

$$\begin{aligned} a(T,\mu_a,g) = \frac{\pi^2}{45}\left[8 + \frac{21}{4}n_f + \frac{45}{2\pi^2}\sum_{a=1}^{n_f}\left(\frac{\mu_a^2}{T^2} + \frac{\mu_a^4}{2\pi^2T^4}\right)\right] - \frac{8}{144}g^2\left[3 + \frac{5}{4}n_f + \frac{9}{2\pi^2}\sum_{a=1}^{n_f}\left(\frac{\mu_a^2}{T^2} + \frac{\mu_a^4}{2\pi^2T^4}\right)\right] \\ - \frac{2}{3\pi}g^3\left[1 + \frac{1}{6}n_f + \frac{1}{6}\sum_{a=1}^{n_f}\left(\frac{\mu_a^2}{\pi^2T^2}\right)\right]^{3/2} \quad , \end{aligned} \tag{10}$$

with T the temperature, V the volume, and g the strong coupling strength taken at a typical momentum $\max(T,\mu_a)$. The sums run over the quark flavors a up to n_f, the total number of contributing flavors. The pressure $p = -(d\Omega/dV)_{T,\mu}$, the entropy $S = -(d\Omega/dT)_{V,\mu}$, etc., follow from the standard thermodynamic relations.

The initial conditions for the hydrodynamic description $\varepsilon_0 = \varepsilon(t_0,\mathbf{r})$ or $p(t_0,\mathbf{r})$, at a specified time $t = t_0$ when the fluid dynamical expansion of the plasma starts, depend sensitively on the preceding space-time evolution during the preequilibrium stage. They are usually guessed on the basis of intuitive estimates.

In contrast with the ideal gas approximation, in this paper the equation of state will be established for which the initial conditions for fluid dynamics will be computed from the characteristics of the preequilibrium dynamics by performing realistic simulations of $A+A$ collisions on the basis of the transport equation (1).

B. Space-time evolution in the Bjorken picture versus the parton cascade model

For the purpose of illustration and to compare the model calculations of this work with the common understanding of the space-time evolution of highly relativistic nuclear collisions, recall the standard picture of a central nuclear collision in the center-of-mass frame during the first few fm/c [21,16,28]. The two Lorentz-contracted nuclei, which may be imagined as two pancake-shaped parton clouds, interpenetrate and deposit a considerable amount of their initial kinetic energy in interactions among the quanta. A short time ($\simeq$1–2 fm/c) after the maximum nuclear overlap at $t = 0$ fm/c and $z = 0$ fm (the center of mass), the two pancakes will recede from the collision point with the speed of light, containing a considerable but reduced amount of the baryon number of the initial nuclei. The central region between the pancakes will quickly materialize into individual excitations of quarks and gluons. This produced quark-gluon matter is almost at rest and eventually develops into an equilibrium state, forming a hot plasma which further on expands and cools until it freezes out to yield the final hadrons [32].

Within this picture, the Bjorken model [21] presumes that from the point of time when equilibration is attained, the expansion of the system proceeds exclusively in longitudinal direction along the beam (z) axis and is invariant under Lorentz boosts along this axis. This implies that all local thermodynamic quantities are functions of the proper time $\tau = \sqrt{t^2 - z^2}$ only, i.e., $\varepsilon(t, \mathbf{r}_\perp, z) = \varepsilon(\tau)$, $T(t, \mathbf{r}_\perp, z) = T(\tau)$, etc. The fluid four-velocity is taken to be $u^\mu(r) \equiv (\gamma, \gamma\mathbf{v}) = (t/\tau, 0, 0, z/\tau)$, so that $v_z = z/t$. Another assumption of the Bjorken scenario is that the baryon number of the initial nuclei is assumed to reside completely in the receding beam fronts and that the central region is ideally baryon-free. Moreover, residual interactions between the partons are neglected and the particles are treated as massless, so that the system can be treated within the ideal-gas approximation. Hence, if one concentrates on the central region and sets in Eq. (10) $g = 0$ and $\mu_a = 0$, one obtains, from (9) with $a(T, \mu_a = 0, g = 0) \equiv a(T)$ the equation of state for an ideal gas of noninteracting, massless quarks and gluons,

$$p = a(T)\, T^4 \tag{11}$$

and, for the energy density, entropy density and particle-number density, respectively,

$$\begin{aligned} \varepsilon &= 3p \left(1 + \frac{T}{a(T)} \frac{\partial a(T)}{\partial T}\right) \simeq 3\, a(T)\, T^4, \\ s &= \frac{\varepsilon + p}{T} \simeq 4\, a(T)\, T^3, \\ n &= b(T)\, T^3, \end{aligned} \tag{12}$$

where

$$a(T) = \frac{\pi^2}{90}\left(16 + \frac{21}{2} n_f\right) = \begin{cases} 4.06\ (n_f = 2), \\ 5.20\ (n_f = 3), \\ 6.36\ (n_f = 4), \end{cases}$$

$$b(T) = \frac{\zeta(3)}{\pi^2}(16 + 9 n_f) = \begin{cases} 4.14\ (n_f = 2), \\ 5.24\ (n_f = 3), \\ 6.33\ (n_f = 4). \end{cases} \tag{13}$$

In (13) $n_f = n_f(T)$ is the effective number of quark flavor degrees of freedom in the deconfined phase at high temperatures $T >$200 MeV.

The equation of state (11) is to be supplemented by initial conditions for a hydrodynamical expansion, which in the Bjorken scenario are crudely estimated as $\varepsilon_0 = \varepsilon(\tau_0) \approx 1 - 10$ GeV/fm^3 and $p_0 = p(\tau_0) \approx \varepsilon_0/3$ at a proper time $\tau_0 \simeq 1$ fm/c after the moment of maximum nuclear overlap at $\tau = 0$ fm/c and $z = 0$ fm.

The aim of this work is to test these assumptions and to check how realistic is the Bjorken scenario for the early space-time evolution of ultrarelativistic nuclear collisions. I will examine these questions by presenting results obtained from simulations of Au + Au collsions on the basis of the parton cascade model. In particular, the model calculations account (among many other features) for (i) finite, flavor-dependent quark masses, (ii) interactions among the quarks and gluons within the framework of perturbative QCD, (iii) chemical potentials for the light quarks which are effectively represented by the valence quark distributions, resulting in a decreasing (with time), but nonvanishing baryon density in the central region, (iv) the dynamically determined, space-time-dependent momentum distributions and the relative admixtures of the gluons and the various quark flavors.

For the remainder of this section, I would like to recall the important role of the entropy production in the context of quantitatively observing the formation of quark-gluon plasmas at the end of the preequilibrium stage of nuclear collisions. First of all, the entropy is independent of the equation of state and the initial conditions for hydrodynamics, because it is produced during the preequilibrium stage and reaches its final value when the system equilibrates, i.e., before the conditions for hydrodynamical description are satisfied. The amount of entropy is conserved through the subsequent hydrodynamical evolution [21]. Introducing the natural variables for the space-time evolution, namely, the momentum rapidity,

$$\begin{aligned} y &= \frac{1}{2} \ln\left(\frac{E + p_z}{E - p_z}\right), \\ p^\mu &= (p_\perp \cosh y, \mathbf{p}_\perp, p_\perp \sinh y), \end{aligned} \tag{14}$$

and the space-time rapidity

$$\begin{aligned} \eta &= \frac{1}{2} \ln\left(\frac{t + z}{t - z}\right), \\ r^\mu &= (\tau \cosh\eta, \mathbf{r}_\perp, \tau \sinh\eta)\ . \end{aligned} \tag{15}$$

the total entropy produced by the partons contained in an interval Δy around $y = 0$ at a given time is obtained

by integrating the local entropy density $s(r)$ from Eq. (4) over position space:

$$S(t) = \int dz \int d^2r_\perp \, u^\mu \, s_\mu$$
$$\simeq \pi R_A^2 \int_{-\Delta y/2}^{+\Delta y/2} d\eta \, \tau \, s(\tau)$$
$$= \Delta y \; \pi R_A^2 \; 4 \, a \, T^3 \, \tau, \tag{16}$$

where $a \equiv a(T)$ from Eq. (13), $T = T(\tau)$, $R_A = 1.14 \, A^{1/3}$ is the nuclear radius and the range of η is given by $-\Delta y/2 \leq \eta \leq +\Delta y/2$. Note that the approximate equality on the right-hand side of (16) holds only under the assumptions of ideal longitudinal flow and of a homogeneous density in transverse direction up to R_A, that is, $s(r) = s(\tau, \eta, \mathbf{r}_\perp) \to s(\tau)$. I emphasize here that in the model calculations within the parton cascade model, the quantity S will be calculated exactly instead.

An important consequence of the thermodynamic equations (4) is the conservation of the total entropy:

$$\frac{d}{d\tau}\left(\frac{dS}{dy}\right) = 0 \quad . \tag{17}$$

In order to relate S to observables, one has to assume that the further evolution following the quark-gluon phase proceeds adiabatically through the mixed parton-hadron phase and that the decoupling of final hadrons is also adiabatic [10,11,15]. If there is a first-order phase transition at a critical temperature T_c, the ratio of the entropy density in the pion plasma, $s^{(\pi)}$, to that of the quark-gluon plasma, $s^{(qg)}$, can be estimated from the effective number of degrees of freedom in the two phases as [21]

$$r \equiv \frac{s^{(\pi)}(T_c)}{s^{(qg)}(T_c)} \approx 0.7 \pm 0.2 \quad . \tag{18}$$

Under these assumptions the total produced entropy can be measured by

$$\frac{dS}{dy} = c^{(qg)} \left(\frac{dN^{(qg)}}{dy}\right)_{b=0} \approx \frac{c^{(\pi)}}{r} \left(\frac{dN^{(\pi)}}{dy}\right)_{b=0} , \tag{19}$$

where, for the case of an ideal gas of partons, respectively, pions,

$$c^{(qg)} = \frac{\pi^4}{45\zeta(3)} \left(\frac{16 + \frac{21}{2} n_f}{16 + 9 n_f}\right)$$
$$= \begin{cases} 3.92 \; (n_f = 2), \\ 3.98 \; (n_f = 3), \\ 4.02 \; (n_f = 4), \end{cases} \tag{20}$$
$$c^{(\pi)} = \frac{\pi^4}{45\zeta(3)} \simeq 3.60 \quad .$$

Conversely, if the amount of entropy produced per unit rapidity is known, then from (18)–(20) the multiplicity of final pions can be predicted:

$$\left(\frac{dN^{(\pi)}}{dy}\right)_{b=0} \simeq (0.19 \pm 0.06) \, \frac{dS}{dy} \quad . \tag{21}$$

In (19) and (21) $b = 0$ indicates zero impact parameter and $dN^{(qg)}/dy$ refers to the number of partons per unit rapidity whereas $dN^{(\pi)}/dy$ is the pion multiplicity at $b = 0$. For the case of variable impact parameter, the multiplicity averaged over all impact parameters, $N^{(\pi)}(b)$, has a geometrical factor $(\pi R_A^2)^2/\pi(2R_A)^2$, whereas the multiplicity at $b = 0$ is proportional to πR_A^2. Therefore the height of the observed rapidity plateau, averaged over all b, is

$$\frac{dN^{(\pi)}}{dy} = \frac{1}{4}\left(\frac{dN^{(\pi)}}{dy}\right)_{b=0} . \tag{22}$$

To summarize the essential points: The total produced entropy contained in an interval dy around $y = 0$ is effectively related to the observable pion multiplicity $dN^{(\pi)}/dy$ via Eqs. (21) and (22). Therefore the multiplicity of pions from the plasma can be predicted by computing the entropy produced by the partons in the central collision region, which in turn can be independently measured. However, the assumption of a quasiadiabatic expansion of quark-gluon plasma and pion gas and the neglect of further produced entropy in the hadronization process are clearly approximations. Nevertheless, if the amount of entropy produced in the central region is large, and in this work it turns out to be enormous, then these effects should be comparably insignificant.

III. PRACTICAL DETAILS OF THE PHASE-SPACE ANALYSIS

Before presenting the results of the model calculations, I would like to explain the methods I used to analyze the nuclear collisions in terms of the time evolution of the parton distributions in six-dimensional phase space. The statistical description of the reaction dynamics in phase space is based on a discretization of the latter and the extraction of the parton distributions. The concept is similar in spirit to earlier phase-space analyses within microscopic models of nuclear dynamics [33,34]. To calculate the distribution functions $F_a(r,p)$ of the partons, the six-dimensional phase-space volume is divided into cells labeled by an index k. The number of partons of type a, $n_a(k)$, in each cell is found at some fixed time in the total center-of-mass frame of the colliding nuclei. Statistics are improved by summing $n_a(k)$ over several collision events of the parton cascade simulation. The distribution functions $F_a(r,p)$ are then estimated as

$$\bar{F}_a(k) = \frac{1}{\nu_{\rm ev}} \left(\frac{n_a(k)}{\Delta\Gamma_a(k)}\right) \quad , \tag{23}$$

where $\nu_{\rm ev}$ is the number of collision events accumulated and

$$\Delta\Gamma_a(k) = \gamma_a \int_k \frac{d^3r \, d^3p}{(2\pi)^3} \tag{24}$$

is the phase-space volume of cell k in natural units ($\hbar = c = 1$) of the elementary volume $h^3 = (2\pi\hbar)^3 \equiv (2\pi)^3$ for partons of species a with degeneracy factors $\gamma_g = 16$ for gluons and $\gamma_q = \gamma_{\bar{q}} = 6$ for each quark flavor.

As has been pointed out in Ref. [33], the division of phase space into cells must be done with some care. There are two essential requirements for an appropriate phase-space discretization.

(i) The cell size must be small enough so that $\bar{F}(k)$ is approximately uniform within the six-dimensional volume of the cells. A too large cell size underestimates the particle density and overestimates the entropy.

(ii) In the average the cells must include enough particles so that the statistical errors in the particle numbers $n(k)$ are not significant. If, for a given cell size, the number of particles is too small such that most cells are empty and the occupied cells contain only very few particles, then the density in cells containing particles overestimates the true density. Since only the occupied cells contribute in the calculation of the entropy, the computed value of the latter would be too low.

To choose a phase-space division that satisfies these two conflicting requirements such that the computed entropy is estimated with sufficient accuracy, it is important to quantitatively understand the errors associated with a certain cell configuration and the number of particles involved in the analysis. The effect of the nonuniformity of F within the cells and the error due to counting statistics with a finite number of particles can be examined with a simple model problem. Consider a spatially uniform, nondegenerate system of N classical particles in a volume V with an isotropic momentum distribution, such that, at a fixed point of time,

$$F(\mathbf{r},\mathbf{p}) = f_0\, e^{-p/a} \ , \tag{25}$$

where $f_0 \propto N/V$ and $p \equiv |\mathbf{p}| = \sqrt{E^2 - m^2}$. Since for a classical nondegenerate system of particles the entropy four-flow given in (2) reduces to

$$s^\mu(\mathbf{r}) = -\int \frac{d^3p}{(2\pi)^3 p^0}\, p^\mu\, F(\mathbf{r},\mathbf{p}) \Big(\ln F(\mathbf{r},\mathbf{p}) - 1 \Big) \ , \tag{26}$$

the total entropy per particle S/N for the phase-space distribution (25) is

$$\frac{S}{N} = \frac{\int d^3r\, s_\mu(\mathbf{r}) u^\mu(\mathbf{r})}{\int d^3r\, n_\mu(\mathbf{r}) u^\mu(\mathbf{r})} = 4 - \ln(f_0) \ , \tag{27}$$

where u^μ is the flow velocity and n^μ the particle four-flow as defined in Eqs. (3) and (2), respectively.

This result is to be compared with the estimate obtained by dividing phase space into cells of volume $\Delta\Gamma(k) = (\Delta^3r\Delta^3p)_k/(2\pi)^3$. Choosing $\Delta r = \kappa V$ and $\Delta p = \xi\, a$ the estimated entropy per particle is

$$\left(\frac{S}{N}\right)_{\rm est} = 1 - \frac{\sum_k \Delta\Gamma(k)\, \bar{F}(k) \ln \bar{F}(k)}{\sum_k \Delta\Gamma(k)\, \bar{F}(k)}$$
$$= 1 - \ln(f_0) + 3\ln(\xi) - \frac{1}{2}\left\{ \sum_{k=0}^{\infty} g(k) \ln\left(\frac{g(k)}{k^2 + k + 1/3} \right) \right\} \ , \tag{28}$$

with

$$g(k) = e^{-k\xi} \Big\{ (1 - e^{-\xi}) \Big[k^2\xi^2 + 2k\xi + 2 \Big] - \xi e^{-\xi} \Big[(2k+1)\xi + 2 \Big] \Big\} \tag{29}$$

and $\sum_k g(k) = 2$. Since only occupied cells contribute to the cellular entropy and a spatially uniform distribution is assumed, the expression (28) does not depend on the spatial cell size Δ^3r, whereas the momentum space division leads to the infinite sum in the last term which explicitly depends on the resolution parameter $\xi = \Delta p/a$. The difference between Eqs. (27) and (28) gives the absolute error $\Delta(S/N) = |S/N - (S/N)_{\rm est}|$ due to the cellular phase space. Its magnitude is displayed in Fig. 1 as a function of ξ. The behavior of $\Delta(S/N)$ with increasing ξ and its small magnitude show that the entropy is a rather smooth function of F. For example, for $\xi = 1$, corresponding to a ratio of particles e in adjacent cells, the absolute error per particle is only 0.04. Aiming at computing the entropy to an accuracy of 0.1 per particle one therefore can permit cell configurations that have F varying by about a factor of 2.5 between neighboring cells. It is worth noting that this behavior agrees with the result of a similar investigation for the simplified case of a one-dimensional phase space [33] as opposed to the six-dimensional example considered here.

The next point is the fact that in practice one deals with a finite number of particles, so that the number of occupied cells is generally smaller than the total number of cells of the covered phase-space, depending on the interplay between the density of particles and the chosen cell size. There is a systematic bias in estimates based on Eq. (23) with $n(k)$ being small. This error, due to counting statistics with a finite number of particles, results in underestimating the entropy. The statistical fluctuations

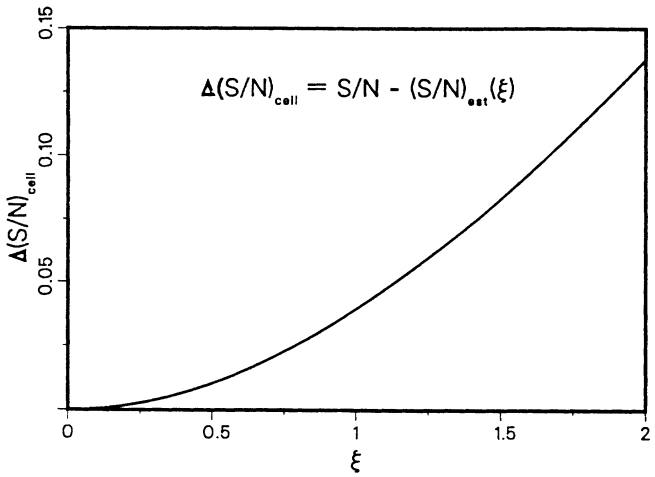

FIG. 1. Absolute error $\Delta(S/N)$ in the entropy per particle due to discretizing phase space in the case of a spatially uniform system of classical particles with momentum distribution (25). The cell size in momentum space depends on the resolution parameter $\xi = \Delta p/a$ via Δp and a was chosen to be 1 GeV/c.

associated with too few particles lead to a too high density in cells containing particles. Since only these cells contribute to $\sum_k \Delta\Gamma\, \bar{F}(k) \ln \bar{F}(k)$, the entropy would be estimated too low from Eq. (23). This error is straightforward to determine by treating the fluctuations in $n(k)$ about the mean $\langle n(k)\rangle$ with Poisson statistics. Following Ref. [33], the average deviation of the statistical estimate from the true cellular entropy is

$$\Delta\left(\frac{S}{N}\right)_{\rm stat} = \frac{\langle \sum_k \{ \langle n(k)\rangle \ln\langle n(k)\rangle - n(k)\ln n(k)\}\rangle}{\sum_k n(k)} = -\frac{\langle 2\sum_k n(k)\, \ln[1+\delta n(k)/\langle n(k)\rangle]\rangle}{\sum_k n(k)}\ , \tag{30}$$

where $\delta n(k) = n(k) - \langle n(k)\rangle$. Expanding the logarithm to second order and using $\langle \delta n(k)^2\rangle = \langle n(k)\rangle$ gives

$$\Delta\left(\frac{S}{N}\right)_{\rm stat} \simeq -\frac{1}{2}\frac{\sum_k 1}{\sum_k n(k)} = -\frac{1}{2}\frac{n_{\rm occ}}{\nu_{\rm ev} N}\ . \tag{31}$$

Here $n_{\rm occ}$ stands for the number of occupied cells and $\nu_{\rm ev} N$ is the total number of particles accumulated in $\nu_{\rm ev}$ events. This implies that, in order to compute the entropy to a reasonable accuracy, the requirement of a sufficiently large number of particles to have good statistics is very moderate. For example, to achieve an accuracy of 0.1 per particle, one needs only an average of five particles in each occupied cell.

To check whether or not these considerations of errors associated with the cellular phase space and the number of particles distributed over it are also true for the practical computation of the entropy of partons in heavy-ion collisions, I studied the previously considered system of particles with the phase-space distribution (25) numerically. The particles were confined inside a cylindrical volume of length 2 fm and radius 4 fm, i.e., $V_{\rm box} \simeq 100$ fm^3, and distributed homogeneously throughout this volume. The parameter a in the distribution (25) was chosen to be 1 GeV/c. Figure 2 shows the absolute error in the entropy per particle for this system as a function of the cell size (in units of Planck's volume h^3) for various numbers of particles N =200–50 000. In accordance with the above considerations, the effect of the number density on the error is far less important than the choice of the cell size. Obviously an accuracy of 0.1 per particle can be achieved with a cell size of $\approx 4h^3$ and a total number of particles $N \geq 2500/\nu_{\rm ev}$, accumulated in $\nu_{\rm ev}$ events, or, an average particle density of $N/V_{\rm box} \geq 25/\nu_{\rm ev}$ fm^{-3}.

Aside from this statistical bias, there will be an additional uncertainty due to fluctuations of the computed S about the mean. For the Monte Carlo simulation of nuclear collisions within the parton cascade model this error can be determined only "experimentally" by simulating a number of collision events and generating an ensemble of computed entropies. It turns out that this error is of the order of 10^{-3} per particle and hence is neglectable. The statistics of the simulations is so good, because in the Au + Au collisions considered in Sec. IV the numbers of particles that contribute to the entropy production are between about 9000 and 20 000 per collision event for $\sqrt{s} = 200A$–$6300A$ GeV.

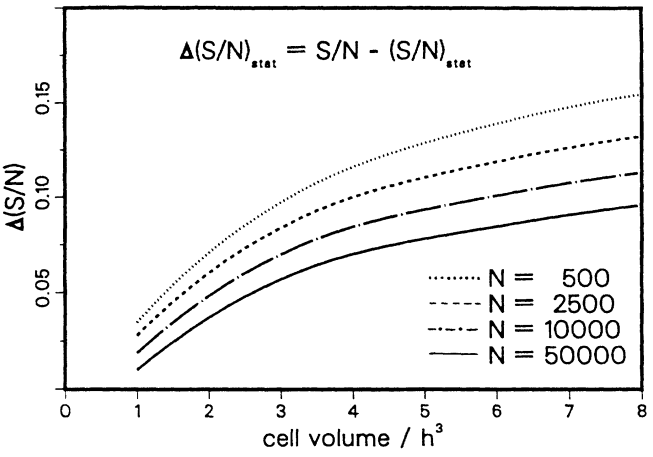

FIG. 2. Absolute error in the entropy per particle as a function of phase-space cell size (in units of h^3), resulting from counting statistics with a finite number of particles. The curves correspond to a system with a total number of N = 200–50 000 classical particles with the momentum distribution (25), spatially confined in a cylinder of 2 fm in length and 4 fm in radius, i.e., a volume of $\simeq$ 100 fm^3.

Finally there is the question of how the time evolution of the produced entropy is affected by the cell division and the particle configuration. This is of interest because the time span for the relaxation of the entropy production determines the equilibration time scale. In the case of nuclear collisions as studied in Sec. IV, the initially sparsely populated phase space will be rapidly filled with partons that are "freed" during the collisions. Therefore one may expect that the statistical error in computing the entropy at given time steps is relatively large in the beginning and decreases as more and more particles are produced, improving the statistics. Thus, the entropy would be underestimated most drastically in the early stage and consequently the rise of produced entropy with time would be too steep. As far as the choice of the cell size is concerned, one would expect that with a too coarse grained phase space it appears to take longer for the system to thermalize. Fortunately, these effects are not very significant, as can be examined quantitatively from the simple system of particles in the cylindrical box considered before. To study the time evolution of the entropy, at time $t = 0$ fm/c the particles were initially distributed inside a very small volume V_0 =0.01 fm^{-3} $\ll V_{\rm box}$ localized in the center of the box. The momentum distribution was sampled from the distribution (25) with $a = 1$ GeV/c as before. The direction of the particles momenta was chosen isotropically. As time proceeds the particles spread out in random directions until they collide with the walls of the box and are reflected. No collisions between the particles are considered. The highly compressed initial particle configuration expands and, after some time, approaches a thermal equilibrium of an ideal gas. The time scale for this equilibration can be estimated from the relaxation of the entropy production as computed from Eqs. (26) and (27). In Fig. 3 the time evolution of the estimated specific entropy $(S/N)_{\rm est}(t)$ for this toy model is shown

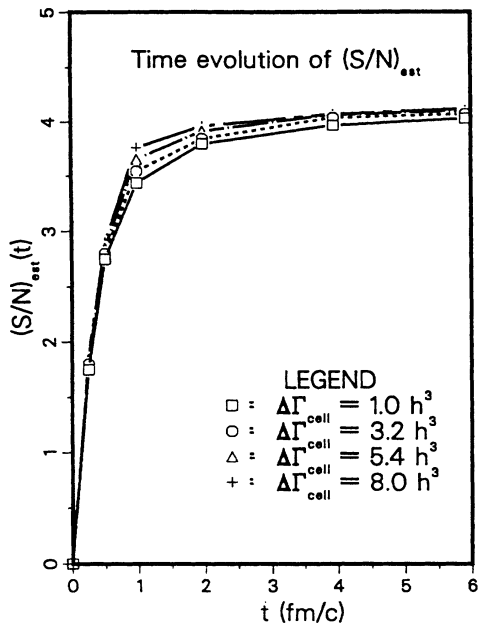

FIG. 3. Time evolution of the entropy production of $N = 10\,000$ noninteracting particles, expanding isotropically from the center of a cylindrical volume $\simeq 100$ fm^3. The particles, initially distributed according to the distribution (25), progressively populate phase-space with time to finally fill out uniformly the volume of the cylinder.

for a total of $N = 10\,000$ particles and various cell sizes $\Delta\Gamma = 1\,h^3 - 8\,h^3$. The entropy per particle is initially zero (because all the particles are assigned to reside in the central cell), rises steeply as the particles spread out to occupy the phase space, and finally reaches its equilibrium value. The curves corresponding to the various phase-space divisions differ insignificantly, except around $t = 1$–2 fm/c, where the curvature is the largest. The relaxation times range from $\simeq 0.5$ fm/c ($\Delta\Gamma = 1\,h^3$) to $\simeq 0.6$ ($\Delta\Gamma = 8\,h^3$), implying a rather small variation of $\simeq 0.1$ fm/c compared to the total equilibration time of about 6 fm/c, that is, a relative error of $\simeq$ 1–2 percent.

IV. CENTRAL Au+Au COLLISIONS AT $\sqrt{s}$=200A–6300A GeV

To study the space-time evolution of the partons and their thermodynamics in ultrarelativistic $A + A$ collisions during the first few fm/c, I performed a series of Monte Carlo simulations of Au + Au collisions ($A = 197$) with various beam energies $\sqrt{s} = 200A, 1000A, 2000A, 4000A, 6300A$ GeV, using the parton cascade model described in Refs. [27,28]. All simulations were carried out with zero impact parameter. The following analysis focuses on the dissipative dynamics of partons in the central collision region during the preequilibrium stage and the eventual formation of a thermalized quark-gluon plasma state. The frame of reference is the center of mass of the colliding nuclei. The system of partons is followed in real time as measured with respect to the center of mass, from the moment the nuclei begin to overlap, $t_i = 0$ fm/c, until a time $t_f = 3$ fm/c when the calculations have been stopped. The microscopic kinetics of the partons during this early time have been studied in detail in Ref. [28], where it was found that the general features of the collisions can be summarized as follows: It takes about a time of $t_0(\sqrt{s}) \simeq 1$–0.4 fm/c (for $\sqrt{s} = 200A$–$6300A$ GeV) from the first touch of the projectiles until the nuclei are practically on top of each other [35]. At $t = 2.5$–3 fm/c the reactions among the partons have essentially faded out, as can be concluded from the number of interactions and the negligible further time variation of the partons' momentum distributions [28]. At $t_f = 3$ fm/c the system looks very much like the picture sketched in Sec. II B. The two beam fronts, which recede from the center of mass with ultrarelativistic speed, contain still a considerable fraction of the baryon number (valence quarks) of the initial nuclei as well as the majority of *primary* gluons and sea quarks that have not interacted but remained spectators throughout. On the other hand, the region in between these beam fronts is strongly populated by "produced" matter, that is, by *secondary* partons that have been set "free" due to scatterings or have been newly created in particle production processes. The produced quark-gluon matter in this central region is essentially at rest. The partons have slowed down considerably from their initially large longitudinal momenta, due to mutual interactions and gluon bremsstrahlung. Although parts of their momenta are redirected in transverse direction, there is no significant global side splash observable during the first 3 fm/c. The system as a whole expands exclusively in longitudinal direction and is characterized by a global one-dimensional flow along the collision axis.

It is this spatial central region on which I will focus in the following; that is, I will be concerned with the time evolution of the secondary partons in a cylindrical central phase-space volume specified below.

A. The phase-space distributions of partons

The distribution functions $F_a(\mathbf{r}, \mathbf{p}, t)$ for the partons species $a = g, q_f, \bar{q}_f$ depend on the six phase-space variables and time. Exploiting the cylindrical symmetry of the dynamical evolution, the spatial coordinates are chosen to be the longitudinal (beam) axis, the transverse direction, and the azimuthal angle, i.e., $\mathbf{r} = (z, r_\perp, \phi_r)$. Similarly, the momentum variables are $\mathbf{p} = (p_z, p_\perp, \phi_p)$. I will consider a *central phase-space volume* which is defined as the composite volume of a cylinder in position space with

$$\begin{aligned} -1\,\text{fm} \le z \le +1\,\text{fm}, \\ 0\,\text{fm} \le r_\perp \le 6.7\,\text{fm} \quad (= R_{\text{Au}}), \\ 0 \le \phi_r \le 4\pi \end{aligned} \tag{32}$$

and a cylinder in momentum space such that

$$\begin{aligned} -5\,\text{GeV/c} \le p_z \le +5\,\text{GeV/c}, \\ 0\,\text{GeV/c} \le p_\perp \le 4.5\,\text{GeV/c}, \\ 0 \le \phi_p \le 4\pi\ . \end{aligned} \tag{33}$$

I will refer to the spatial cylinder (32) also as the *central volume* or the *central region*. This central phase-space volume [the product of (31) and (32)] is divided into six-dimensional phase-space cells with

$$\Delta z = 0.4 \text{ fm} \ , \qquad \Delta r_\perp = 1.5 \text{ fm} \ , \qquad \Delta\phi_r = \frac{\pi}{2}, \tag{34}$$
$$\Delta p_z = 0.5 \text{ GeV/c} \ , \ \Delta p_\perp = 0.3 \text{ GeV/c} \ , \ \Delta\phi_p = \frac{\pi}{2} \ .$$

The parton distributions that are evolved in time according to the transport equation (1) are extracted at certain points of time on the basis of Eq. (23) with respect to this phase-space discretization. It should be noted that the division defined by (34) results in an increasing cell size from the center to the edge of the phase-space volume. A slightly more accurate but less practical cell configuration with equal sized cells could be employed by decreasing the transverse shell thickness of the cylinders in $\mathbf{r}$ and $\mathbf{p}$ space according to the radial distance from the centers. A numerical comparison between such a cell configuration and the one specified by (34) shows a negligible change in the specific entropy $\Delta(S/N) \simeq 0.01$. I also remark that the fluctuations of the particle numbers in the azimuthal bins of the variables ϕ_r and ϕ_p are very small. They vary by less than a percent, which manifests the cylindrical symmetry in both position and momentum space.

As an illustration of the time-dependent shapes of the phase-space distributions, I show in Figs. 4 and 5 two-dimensional projections of the total parton distribution

$$F(\mathbf{r},\mathbf{p},t) = 16\, F_g(\mathbf{r},\mathbf{p},t) + 6 \sum_a \Big\{ F_a(\mathbf{r},\mathbf{p},t) + F_{\bar{a}}(\mathbf{r},\mathbf{p},t) \Big\}, \tag{35}$$

where the factors 16 and 6 are the color × spin degeneracies for gluons and (anti)quarks, respectively, for two

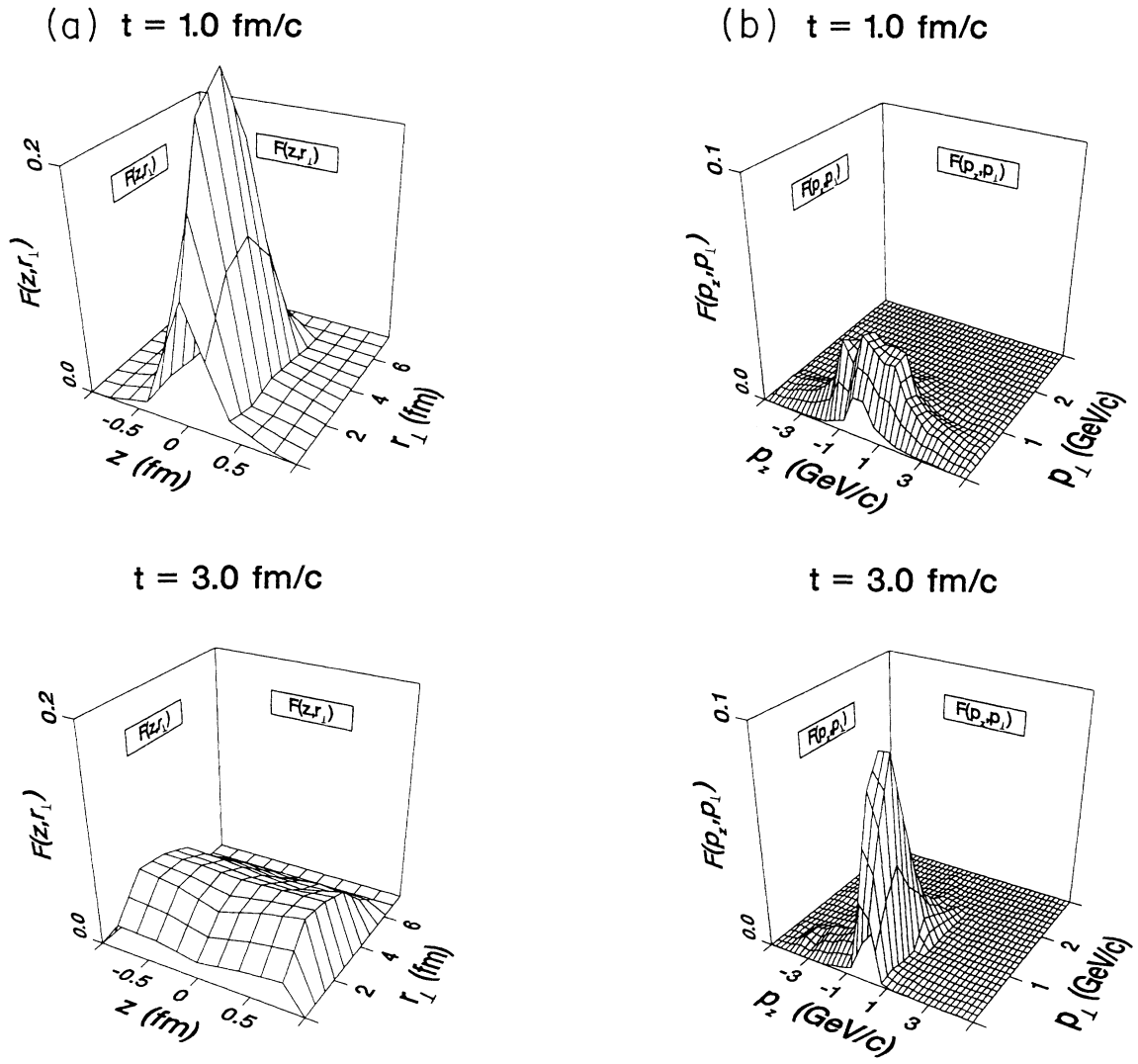

FIG. 4. The projected distributions (36), $F_r(z, r_\perp, t)$ (a) and $F_p(p_z, p_\perp, t)$ (b), of the partons' total phase-space distribution during a Au + Au collision with $\sqrt{s} = 200A$ GeV. Shown are the profiles in the central volume (32) at t =1 fm/c, the moment of maximum nuclear overlap, and at t =3 fm/c, when only the partons with small rapidity remain.

characteristic points of time during a Au + Au collision with $\sqrt{s} = 200A$ GeV. The first is at $t_0 = 1$ fm/c, the moment of maximum overlap and the second is at $t_f = 3$ fm/c when the two fast beam fronts have receded $\simeq 2$ fm from the center of mass and only the matter which has considerably slowed down longitudinally or was produced at low momentum remains in the central region. For these collisions with $\sqrt{s} = 200A$ GeV the total numbers of secondary partons $N(t) = \int d^3r\, d^3p F(\mathbf{r},\mathbf{p},t)/(2\pi)^3$, present in the central phase-space volume, were about $N(t_0) = 8600$ and $N(t_f) = 2100$ per collision event, averaged over five events.

In Fig. 4 the two-dimensional projected distributions in position, respectively, momentum space,

$$F_r(z,r_\perp,t) = \frac{\int d\phi_r\, d^3p\, F(\mathbf{r},\mathbf{p},t)}{\int d^3r\, d^3p\, F(\mathbf{r},\mathbf{p},t)},$$
$$F_p(p_z,p_\perp,t) = \frac{\int d\phi_p\, d^3r\, F(\mathbf{r},\mathbf{p},t)}{\int d^3r\, d^3p\, F(\mathbf{r},\mathbf{p},t)}, \tag{36}$$

are plotted for these two points of time. Note that in transverse direction the distributions are weighted by $r_\perp^{-1}$, respectively $p_\perp^{-1}$, according to the integration over the angles. The spatial distributions F_r [Fig. 4(a)] show that the matter in the central region expands longitudinally from its highly compressed state (t_0 =1 fm/c) to establish a rather homogeneous plateau shape (t_f =3 fm/c), whereas in transverse direction no significant flow is observable so that the Fermi-type shape of the nuclei is very well conserved even at 3 fm/c. From the momentum distributions F_p [Fig. 4(b)] one observes that even at t_0 =1 fm/c, when the distribution still reflects the initial momentum distribution to a good extent, the majority of partons has relatively small longitudinal momenta $|p_z| \leq 3$ GeV/c. At t_f =3 fm/c however, only the slow partons with $|p_z| \leq 1$ GeV/c remain, whereas the faster ones have escaped out of the central region. Parts of the longitudinal momentum are redirected in transverse direction, as is inherent in the exponential shape along

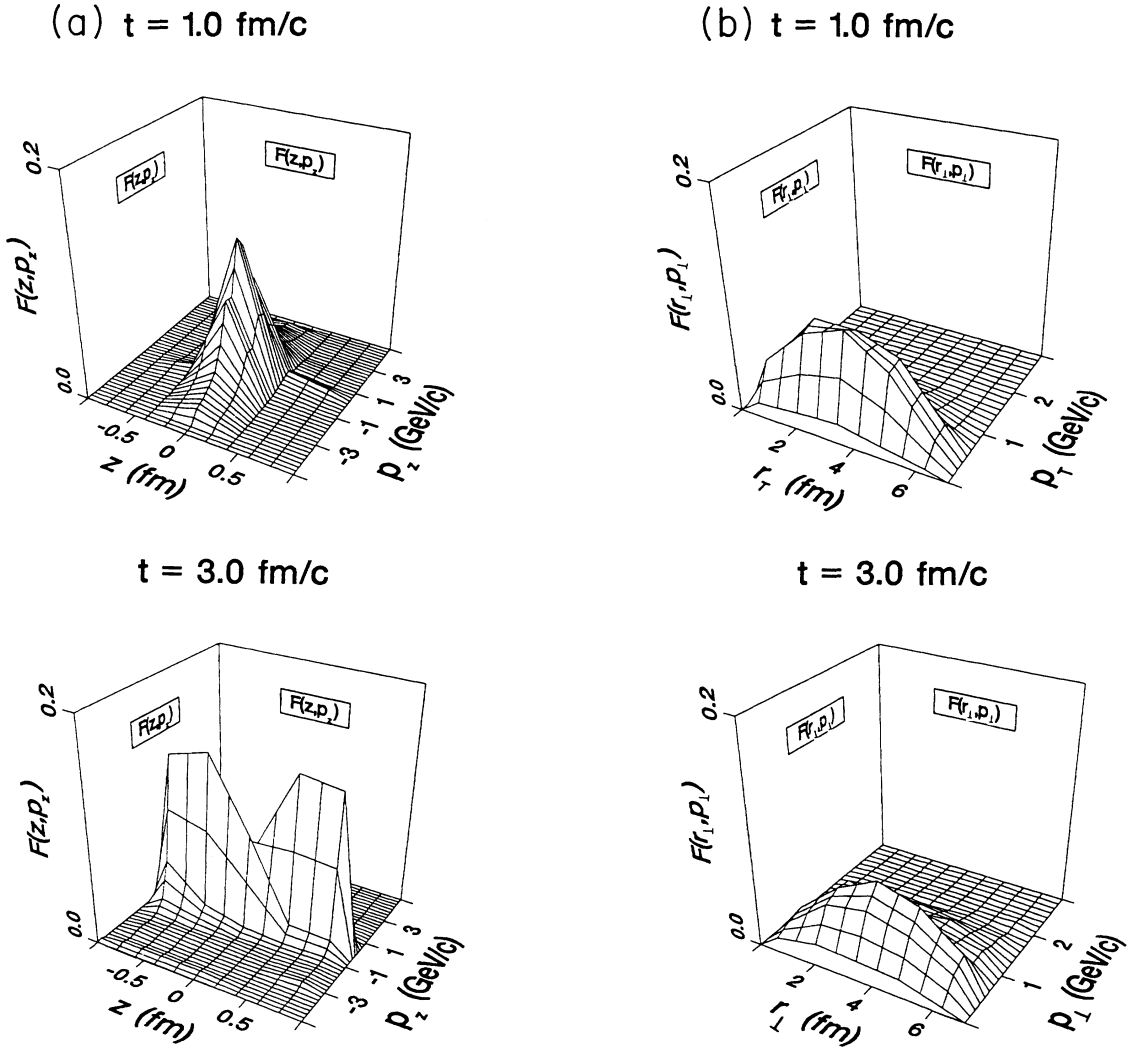

FIG. 5. The projections (37) of the total phase-space distribution of partons, $F_\parallel(z,p_z,t)$ (a) and $F_\perp(r_\perp,p_\perp,t)$ (b), for a Au + Au collision with $\sqrt{s} = 200A$ GeV. The distributions exhibit the correlation between the partons' positions and their momenta t =1 fm/c and t =3 fm/c.

$p_\perp$ with $\langle p_\perp \rangle \simeq 0.65$ GeV/c compared to the $\langle p_\perp \rangle \simeq 0.38$ GeV/c of the initial partons [28]. Also, a large extent of the initial momentum is harnessed for the production of new partons.

To examine the correlation between the partons' positions and momenta, in Fig. 5 the projected distributions

$$F_\parallel(z,p_z,t) = \frac{\int d^2r_\perp\, d^2p_\perp\, F(\mathbf{r},\mathbf{p},t)}{\int d^3r\, d^3p\, F(\mathbf{r},\mathbf{p},t)},$$
$$F_\perp(r_\perp,p_\perp,t) = \frac{\int dz\, dp_z\, d\phi_r d\,\phi_p\, F(\mathbf{r},\mathbf{p},t)}{\int d^3r\, d^3p\, F(\mathbf{r},\mathbf{p},t)} \qquad (37)$$

are displayed corresponding again to the two points of time $t_0 = 1$ fm/c and $t_f = 3$ fm/c. At $t_0 = 1$ fm/c, $F_\parallel$ [Fig. 5(a)] reflects the localized spatial distribution along the z direction with a spread of about 1 fm, correlated with a relative broad distribution in p_z. In strong contrast to that, at $t_f = 3$ fm/c, the occupation probability in z direction is very homogeneous when integrated over p_z, whereas about 75 percent of the partons have longitudinal momentum of less than 0.5 GeV/c. The "V" structure in the range $|z| \leq 0.5$ fm arises from the view angle of the three-dimensional plot. In fact, the distribution is scissor shaped, separating the partons with positive and negative longitudinal momentum. The transverse distribution $F_\perp$ [Fig. 5(b)] remains almost unaffected along $r_\perp$ in between $t_0 = 1$ fm/c and $t_f = 3$ fm/c. Along $p_\perp$, the distribution indicates a moderate amount of transverse momentum production corresponding to the shape of F_p in Fig. 4(b). Actually, between $t_0 = 1$ fm/c and $t_f = 3$ fm/c, the initial Gaussian $p_\perp$ distribution bends out rather drastically, develops a power-law tail, and then relaxes back to an exponential form [27,28].

B. Time evolution of energy, particle, and entropy densities

Having found an appropriate cell configuration for the central phase-space volume defined by (32)–(34), I turn now to the variation of the energy densities, particle densities, and entropy densities produced by secondary partons. For the practical computation of these space-time-dependent quantities certain points of time were selected at which snapshots were taken during the nuclear collisions. At the chosen time steps the spatial profiles of the scalar, invariant local energy density $\varepsilon(\mathbf{r},t)$, the local particle density $n(\mathbf{r},t)$, and the local entropy density $s(\mathbf{r},t)$ were obtained as follows: For each "experiment," the distributions $F_a(\mathbf{r},\mathbf{p},t)$ of gluons ($a = g$) and (anti)quarks ($a = q_f, \bar{q}_f$) of five flavors f were estimated from the corresponding cellular functions $\bar{F}_a$ according to Eqs. (23) and (24) on the basis of accumulated statistics from a number of collision events. In addition the four-momentum of each individual spatial cell k (the sum of four-momenta of the particles in the cell) with respect to the total center-of-mass was computed. In order to calculate the densities ε, n, and s in an invariant manner, the local cellular densities $\bar{\varepsilon}(k)$, $\bar{n}(k)$, and $\bar{s}(k)$ were obtained by boosting from the nuclear center-of-mass to the rest frame of each cell and evaluating these quantities along the formulas (2)–(4) whereby the Lorentz-contracted cell volume associated with its momentum relative to the total center-of-mass was taken into account.

In Fig. 6 the time development of the energy density profile in the central region, obtained in this fashion, is shown for a Au + Au collision at $\sqrt{s} = 200A$ GeV. The maximum energy density in this case is reached at $t \simeq 1$ fm/c around $z = 0$ fm. The first picture in Fig. 6 is therefore already 0.2 fm/c after the maximum density. One observes that the further space-time evolution is at first characterized by a large longitudinal flow of the fast particles which then escape with progressing time from the central region in opposite directions forming two receding fronts. On the other hand, the softer partons expand slowly and eventually establish an isotropic plateau between -1 fm $\leq z \leq 1$ fm and in transverse direction up to $r_\perp \simeq 4$ fm, beyond which the energy density drops significantly.

To analyze the process of local equilibration as a function of time in a quantitative manner, it is elucidating to focus on the time evolution of the energy density and the particle density in a thin disk centered at $z = 0$ fm. For this purpose I define a *central slab* with longitudinal extent and transverse radius

$$-0.2 \text{ fm} \leq z \leq +0.2 \text{ fm}, \qquad 0 \text{ fm} \leq r_\perp \leq 6.7 \text{ fm}, \qquad (38)$$

which is the middle slice of the central volume defined in (31). As is obvious from Figs. 4–6, in this central slab the densities will reach their absolute maximum and will decrease the fastest as the particles move apart, so that a local equilibration in the central slab serves as an indicator for the degree and the time scale of a global thermalization. Also note that at $t_f = 3$ fm/c the local energy density in the central slab (38) is representative for the global density in the whole central volume (32) (with $|z| \leq 1$ fm), as can be seen in the last plots of Figs. 4 and 6. A similar behavior is found for the particle density and the entropy density for all of the considered beam energies. Moreover, the time t measured with respect to the nuclear center-of-mass at $z = 0$ fm in the central slab corresponds to the *proper time* τ, which I define as

$$\tau = \sqrt{(t - t_0)^2 - z^2}\ , \qquad (39)$$

such that $\tau = 0$ fm/c at $t = t_0$, where $t_0 \equiv t_0(\sqrt{s})$ is the energy-dependent point of maximum nuclear overlap [35],

$$t_0(\sqrt{s}) = \begin{cases} 1 \text{ fm}/c\,, \sqrt{s} = 200A \text{ GeV}, \\ 0.75 \text{ fm}/c\,, \sqrt{s} = 1000A \text{ GeV}, \\ 0.55 \text{ fm}/c\,, \sqrt{s} = 2000A \text{ GeV}, \\ 0.45 \text{ fm}/c\,, \sqrt{s} = 4000A \text{ GeV}, \\ 0.40 \text{ fm}/c\,, \sqrt{s} = 6300A \text{ GeV}. \end{cases} \qquad (40)$$

The definition (39) of τ is motivated by the usual choice of requiring the tip of the forward light cone (which bounds the longitudinal expansion) to be at $\tau = 0$ fm/c and $z = 0$ fm [21].

The time evolution and the beam energy dependence

of the energy densities ε, particle densities n, and entropy densities s is exhibited in the Figs. 7–9. Figure 7 displays the time evolution of ε, n, and s in the central slab for Au + Au collisions with $\sqrt{s} = 200A$–$6300A$ GeV. As before, $t_i = 0$ fm/c corresponds to the moment of nuclear contact. The densities rise steeply as the nuclei interpenetrate, reach their maxima between 0.4 fm/c and 1 fm/c [36], and decrease quickly as the matter expands. Figure 8 exhibits the corresponding dependence on the proper time τ, as defined in (39), for the case $\sqrt{s} = 200A$ GeV, for which the decrease of the densities in various slabs $0 \leq |z| \leq 0.2$ fm,..., $0.8 \leq |z| \leq 1$ fm was computed. The different symbols refer to the magnitude of the densities in the slabs along the z axis. The points are obviously clustered around a common curve which I tried to fit to a proper time dependence of $\tau^{-\alpha}$. A similar behavior is found for the higher beam energies, but with an initially faster decrease, as is already obvious from Fig. 7, so that the resulting fit values of α increase as specified below. For comparison, in case of perfect fluid dynamics the points would lie exactly on one curve and the energy density should decrease as $\varepsilon \sim \tau^{-\alpha}$ with $\alpha = 4/3$. For a free

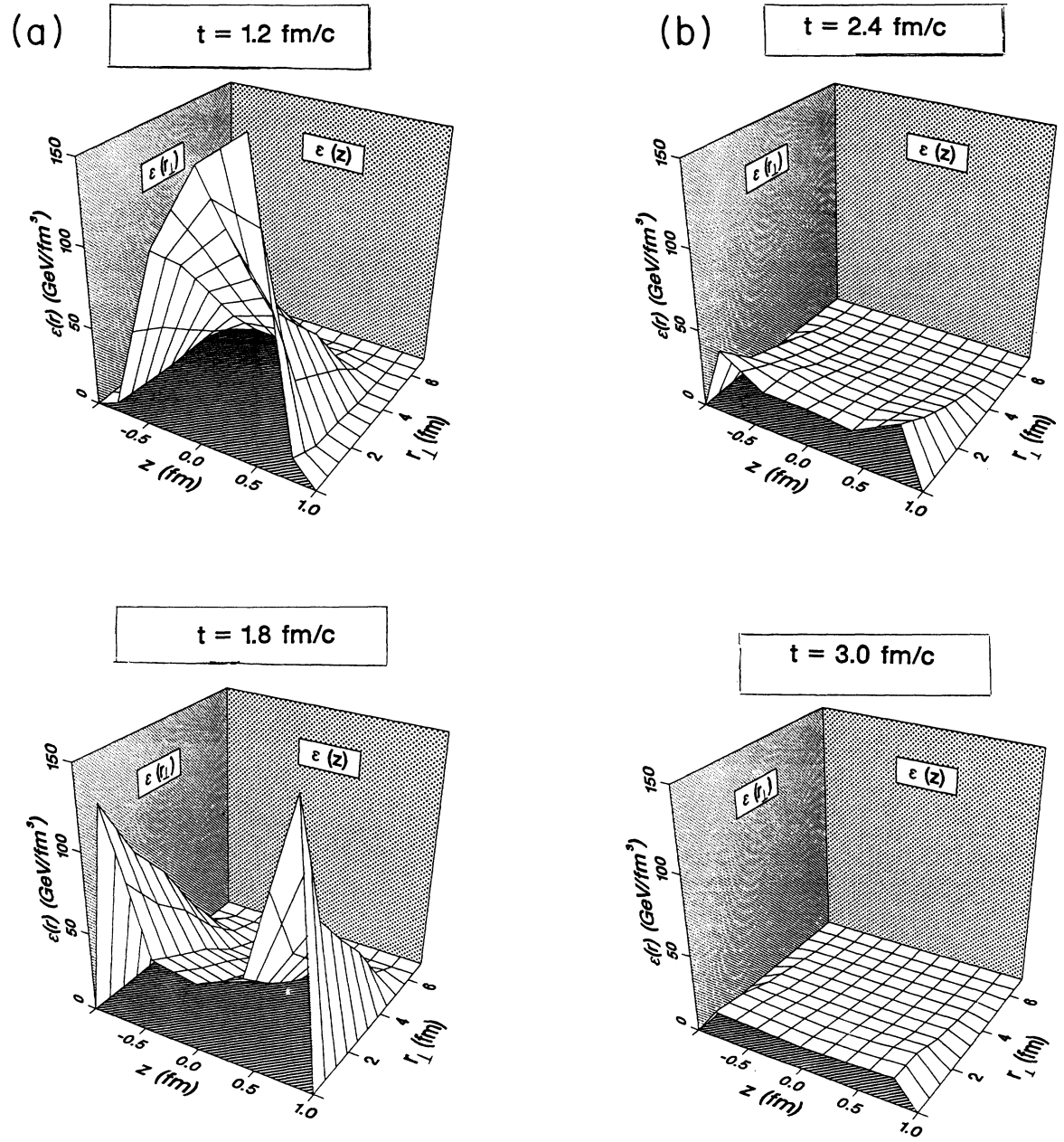

FIG. 6. Time development of the energy density profile in the central region of a Au + Au collision with $\sqrt{s} = 200A$ GeV. The snapshots exhibit the space-time evolution of the energy density of the secondary partons in four characteristic profiles between $t = 1.4$ fm/c ($\simeq 0.4$ fm/c after the maximum density was achieved) and $t = 3$ fm/c. Note that in transverse direction the density profiles are weighted by $r_\perp^{-1}$, i.e., $\varepsilon(r_\perp) = dE/r_\perp dr_\perp$.

streaming system of particles on the other hand $\alpha = 1$. The fact that $\alpha < 1$ in Fig. 8 indicates a continued energy deposition in the central region, due to the finite thickness of the nuclei which results in a smeared-out time variation of the partons' spatial population around $z = 0$ fm. Finally in Fig. 9 the beam energy dependence of the final densities at $\varepsilon(t_f)$ and $n(t_f)$ at $t_f = 3$ fm/c is shown. As stated above, at this point of time the densities are isotropic over about a volume of 2 fm in longitudinal extension and 4 fm in transverse radius.

The most prominent implications of Figs. 7–9 are as follows.

(i) With increasing beam energy $\sqrt{s}$ the absolute maximum of the energy density shows an approximately linear growth. Its magnitude corresponds to about 60 percent of the total center-of-mass energy being contained in the central slab. The maximium values of the particle and entropy densities achieved, on the other hand, roughly increase with a logarithmic dependence. An increase in the beam energy results in earlier times for the maximum energy densities to be achieved and also in a faster relaxation of the system [37].

(ii) The energy, particle, and entropy densities decrease with proper time τ as $\varepsilon \sim \tau^{-\alpha}$, $n \sim \tau^{-\beta}$, and $s \sim \tau^{-\gamma}$, where $\alpha \simeq 0.85 - 1.1$, $\beta \simeq 0.6 - 0.7$, and $\gamma \simeq 0.55 - 0.65$ for $\sqrt{s} = 200A$–$6300A$ GeV. The decrease is the slowest

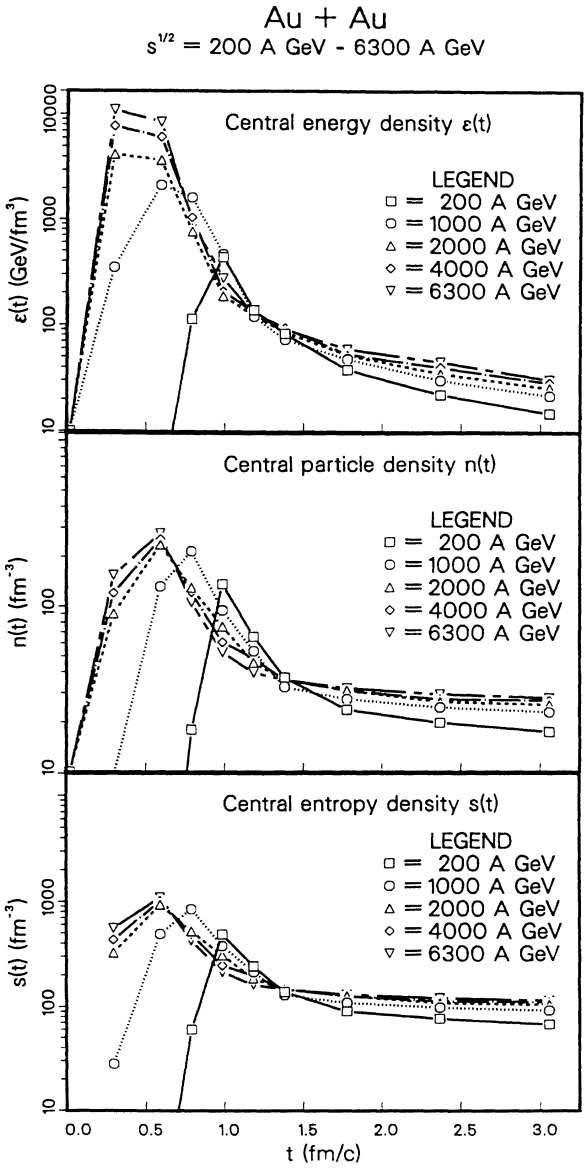

FIG. 7. Time evolution of the central energy density ε, particle density n, and entropy density s in the central slab around $z = 0$ fm, defined by (38), for Au + Au collisions with $\sqrt{s} = 200A$–$6300A$ GeV. Note that for $\sqrt{s} \geq 2000A$ GeV, the exact points of time for the maximum densities to be achieved lie somewhere between the second and third data points.

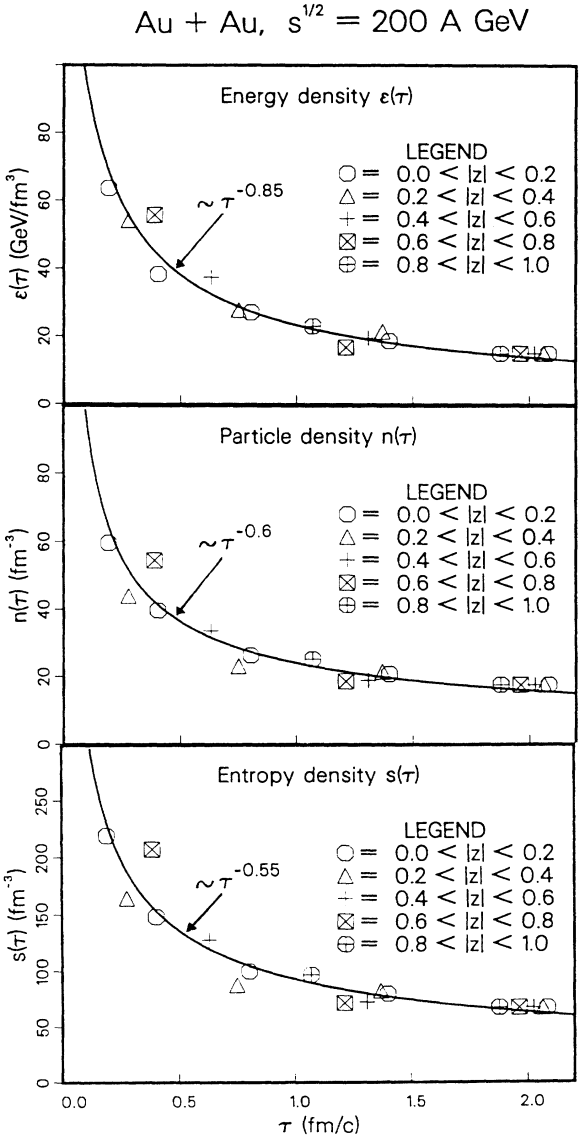

FIG. 8. Decrease of the energy, particle, and entropy density with proper time τ, defined in (39) and (40), in Au + Au at $\sqrt{s} = 200A$ GeV. The symbols correspond to the densities at selected time steps in different slabs along the beam axis, 0 fm $\leq z \leq$ 0.2 fm, ... , 0.8 fm $\leq z \leq$ 1 fm. The full curves are interpolations obtained by trying to fit the clustered points to a $\tau^{-\alpha}$ behavior.

in the central slab ($|z| \leq 0.2$ fm) and becomes faster with increasing distance from the center of mass at $z = 0$ fm. The decrease is slower than what one expexts for a perfect fluid or a free streaming system.

(iii) The final densities at t_f =3 fm/c are still rather large, with ε =15–31 GeV fm^{-3}, n =17.5–28 fm^{-3}, and s =67.5–120 fm^{-3}. Their beam energy dependence can be parametrized as $\varepsilon \simeq 2.3$ GeV fm$^{-3} w^{+0.05} \ln(w)$, $n \simeq 4.0$ GeV fm$^{-3} w^{-0.025} \ln(w)$, and $s \simeq 12.0$ GeV fm$^{-3} w^{+0.015} \ln(w)$, where $w = \sqrt{s}/A$ GeV.

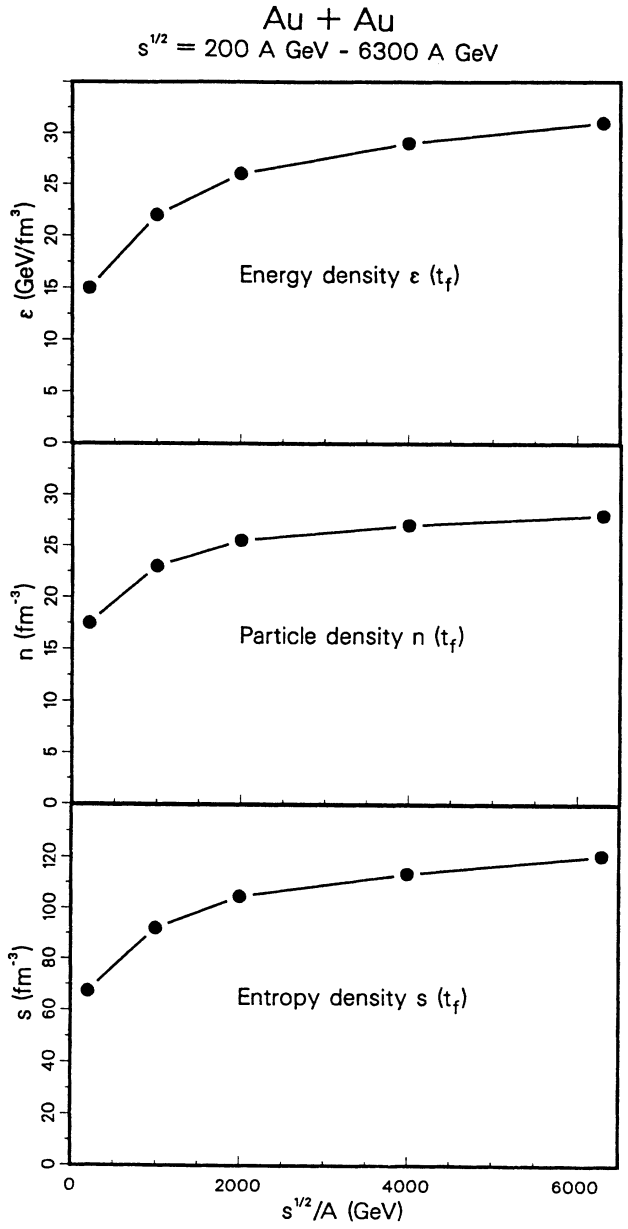

FIG. 9. Beam energy dependence of the final energy, particle, and entropy densities at t_f =3 fm/c when the calculations were stopped. The points are the computed values for the considered beam energies $\sqrt{s} = 200A$–$6300A$ GeV.

C. Entropy production

Next I consider the total entropy S produced by the secondary partons in the central region. Figure 10(a) displays the time development of the specific entropy $(S/N)(t)$ for the various beam energies, whereas Fig. 10(b) shows the corresponding number of particles $N(t)$ present in the central phase-space volume (32) and (33) at time t. The curves show a rapid buildup of S/N and relax approximately exponential to reach their final values between 3.9 and 4.3. Comparing these values with $(S/N)^{\text{ideal}} \simeq 4$ for an ideal gas of noninteracting massless quarks and gluons, one sees that the difference between the resulting entropy of the realistic model calculation and the idealized case amounts only to $\simeq \pm 0.2$–0.3. Although the model includes massive quarks and accounts for interactions among the partons (which however at 3 fm/c have reduced to relatively infrequent, mostly elastic scatterings), the system of partons looks from this point of view effectively like an almost ideal gas. The variation

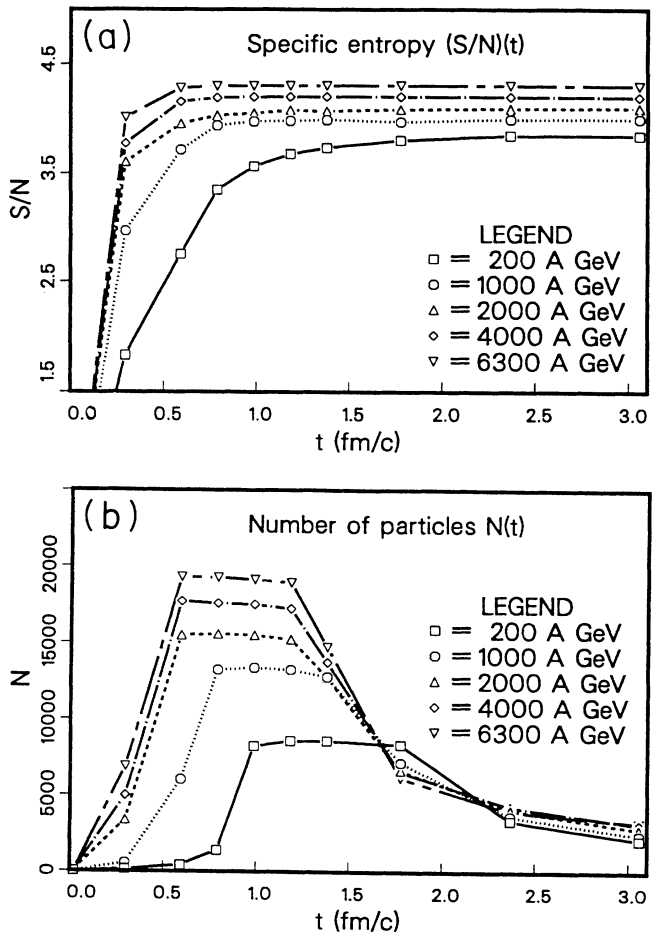

FIG. 10. (a) Increase with time of the total entropy per particle $(S/N)(t)$ produced by the secondary partons in the central region of Au + Au collisions with $\sqrt{s} = 200A$–$6300A$ GeV. (b) Number of particles $N(t)$ present in the central phase-space volume at time t, which contribute to the entropy production shown in (a).

with beam energy is probably due to a weak temperature dependence of the ratio between entropy and the number of partons. As will be shown below, the temperature in the central region grows slowly with the beam energy, so that the effective number of plasma degrees of freedom are expected to increase too [21]. This in turn leads naturally to a larger entropy per particle.

The relaxation times $\tau_{\rm relax}$ (the time it takes to reduce the deviation from the equilibrium value by a factor of e) associated with the entropy production depend significantly on the beam energy in accord with the similar behavior of the time dependence of the densities in Figs. 7 and 8. This beam energy dependence $\tau_{\rm relax}$ is evident in Fig. 11 where $\tau_{\rm relax}$ is plotted versus $\sqrt{s}/A$.

The contents of Figs. 10 and 11 may be summarized as follows:

(i) The entropy per particle produced in the central region is slightly increasing with the beam energy. The resulting final values of S/N at t_f =3 fm/c are 3.87, 4.02, 4.14, 4.21, 4.29 for $\sqrt{s}/A$ =200, 1000, 2000, 4000, 6300 GeV, respectively, which come close to the specific entropy of an ideal noninteracting parton gas with a value of $\simeq$ 4.

(ii) The relaxation times for the various beam energies $\sqrt{s}/A$ = 200A, 1000A, 2000A, 4000A, 6300A GeV are estimated as $\tau_{\rm relax} \simeq$ 0.41, 0.24, 0.18, 0.13, 0.11 fm/c, respectively, and decrease with growing beam energy roughly as $\tau_{\rm relax}^{-1} \sim \ln(\sqrt{s}/A)$.

D. Temperatures

In order to extract the equation of state (Sec. IV E), knowledge of the temperature dependence of the pressure or the energy density is required at a point of time when the system of partons has attained an equilibrium state. The magnitude of the temperature at this point then fixes the initial conditions for a hydrodynamical description of the further space-time evolution, that is, the initial energy density, pressure, temperature, etc., at the time when the fluid dynamical expansion is supposed to start. To measure the temperature associated with the parton distributions in the central phase-space volume, one has to ask how well the corresponding energy, particle, and entropy densities reflect thermalization of the system. Since the temperature is space-time dependent it only makes sense to define this quantity locally through ε, n, or s within the rest frame of a sufficiently small volume in which the matter is approximately thermalized. Therefore, in order to estimate the time variation of the temperature of the produced quark-gluon matter as it expands, I tried to extract local temperatures in the thin central slab, defined in (38), from the time-dependent densities ε, n, and s in this slab. Recall that from the preceding results it appears as if the system approaches a state that effectively exhibits the properties of a perfect gas of quarks and gluons. In analogy to the ideal gas case, one may therefore parametrize the energy, particle, and entropy densities in the central slab in the form of Eq. (12),

$$\begin{aligned} \varepsilon(t)|_{z=0} &= 3\, a(t)\, T^4(t)|_{z=0}, \\ s(t)|_{z=0} &= 4\, a(t)\, T^3(t)|_{z=0}, \\ n(t)|_{z=0} &= b(t)\, T^3(t)|_{z=0} \end{aligned} \tag{41}$$

with

$$a(t) = \frac{27}{256}\left(\frac{s^4(t)}{\varepsilon^3(t)}\right), \quad b(t) = \frac{27}{64}\, n(t)\left(\frac{s(t)}{\varepsilon(t)}\right)^3 . \tag{42}$$

Then the time-dependent central temperature can be estimated by

$$\begin{aligned} T(t)|_{z=0} &= \left(\frac{\varepsilon(t)}{3\,a(t)}\right)^{1/4}_{z=0} \\ &= \left(\frac{n(t)}{b(t)}\right)^{1/3}_{z=0} = \left(\frac{4}{3}\,\frac{s(t)}{\varepsilon(t)}\right)_{z=0} . \end{aligned} \tag{43}$$

The resulting time development of the temperatures $T(t) \equiv T(t)|_{z=0}$ in the central slab for the various beam energies considered is shown in Fig. 12(a). Note that the origin of the t axis is set to t =1 fm/c. In fact, the curves represent effective temperatures at earliest probably from $t \simeq$1.2 fm/c on; before, it does not make sense to speak of temperatures, since the parton distributions are highly nonequilibrated, even in the central slab. At the final time of the calculations, t_f =3 fm/c, the temperatures in the central slab also represent the global temperatures within a volume of about 2 fm in longitudinal extension and about 4 fm in transvere radius, in which the densities of the partons reach a constant value throughout [see Figs. 4(b) and 6]. In Fig. 12(b) the dependence of the final temperatures $T(t_f)$ on the beam energy $\sqrt{s}/A$ is plotted. Also shown are the curves that correspond to the case of an ideal noninteracting gas of massless partons, Eqs. (12) and (13), with the same energy and entropy densities and n_f = 3, 4 quark flavors (dotted lines).

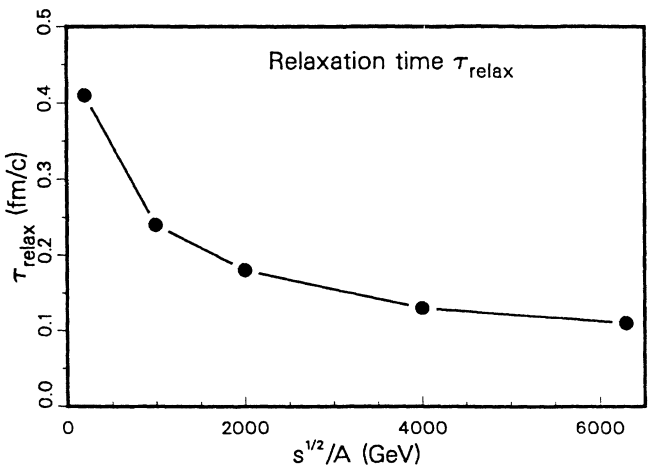

FIG. 11. The relaxation times $\tau_{\rm relax}$ associated with the entropy production shown in Fig. 10(a), as a function of the beam energy. The points are the values estimated from the approximate exponential relaxation of the specific entropy for the considered beam energies $\sqrt{s}$ = 200A–6300A GeV.

The implications of Figs. 12(a) and 12(b) are the following.

(i) The central temperatures at $z = 0$ fm drop relatively slowly for $t > 1.2$ fm/c, approximately $\sim t^{-1/3}$ ($= \tau^{-1/3}$ at $z = 0$ fm). The decrease with time depends only weakly on the beam energy.

(ii) The magnitude of T at $t_f = 3$ fm/c increases slowly with the beam energy, with a logarithmic dependence $\sim \ln(\sqrt{s}/A)$. The final values are $T(t_f) = 297$, 319, 332, 341, 343 MeV for $\sqrt{s} = 200A$, $1000A$, $2000A$, $4000A$, $6300A$ GeV, respectively.

(iii) The fact that $T \sim \ln(\sqrt{s}/A)$ whereas the relaxation time behaves as $\tau_{\rm relax}^{-1} \sim \ln(\sqrt{s}/A)$ (Fig. 11) implies that $T\tau_{\rm relax} \approx$ const—a property that one expects already from the uncertainty principle.

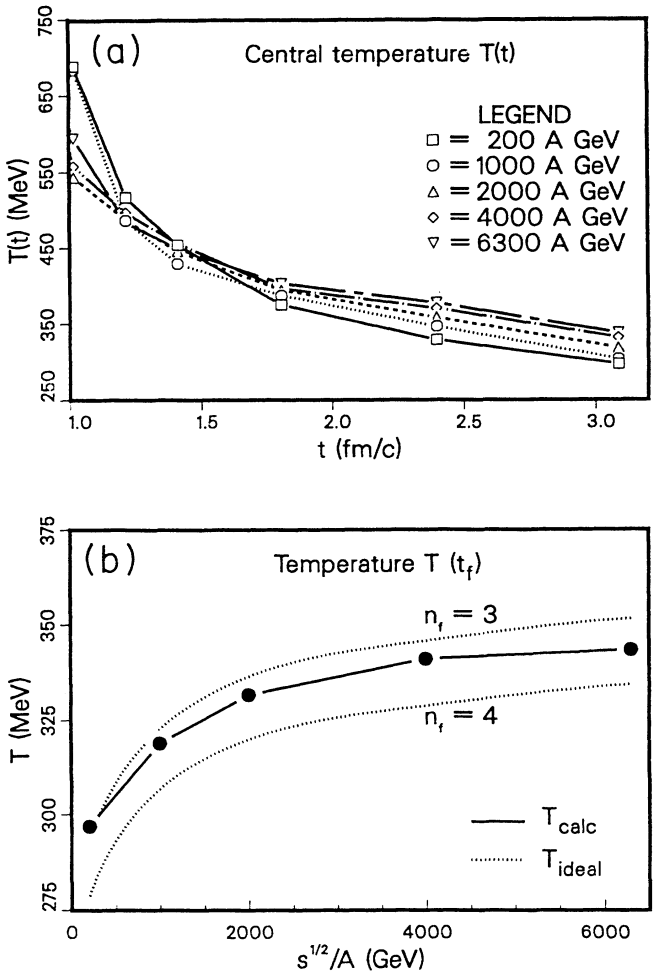

FIG. 12. (a) Decrease with time development of the temperatures $T(t) \equiv T(t)|_{z=0}$ in the central slab for the various beam energies $\sqrt{s} = 200A$–$6300A$ GeV. Note that the origin of the t axis is set to $t = 1$ fm/c, corresponding to a proper time $\tau = 0$–0.6 fm/c for $\sqrt{s}/A = 200$–6300 GeV. (b) Beam energy dependence of the final temperatures $T(t_f)$ ($t_f = 3$ fm/c). The points are the computed values for the considered beam energies $\sqrt{s} = 200A$–$6300A$ GeV. Also shown are the curves that correspond to the case of an ideal noninteracting gas of massless partons, with the same energy and entropy densities and $n_f = 3, 4$ quark flavors (dotted lines).

E. The equation of state and initial conditions for hydrodynamics

Turning to the equation of state associated with the densities ε, n, and s at $t_f = 3$ fm/c, the question is, how well do these densities reflect the degree of thermalization? From the analysis in Secs. IV B–IV D, it appears as if the partons in the central region indeed approach a state of equilibration. To indicate how close these quark-gluon plasmas are to ideal gases of noninteracting massless partons, in Fig. 13 the functions $a(t)$ and $b(t)$ [defined in (41)] are shown for $t = t_f$. Figure 13(a) displays the beam energy dependence of $a(t_f)$ and $b(t_f)$. In addition the dimensionless quantity $\varepsilon^{3/4}/n = (3a)^{3/4}/b$ is plotted. Obviously, there is a moderate increase of $a(t_f)$ as one proceeds to larger energies, whereas $b(t_f)$ is almost

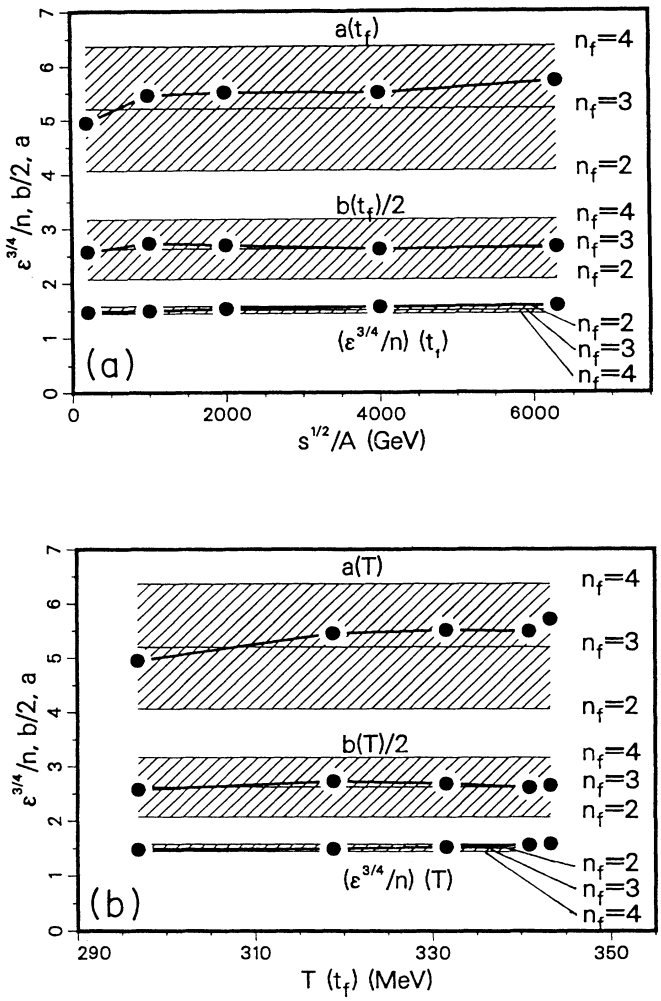

FIG. 13. The functions $a(t)$ and $b(t)$ defined in (41), as well as the dimensionless ratio $\varepsilon^{3/4}/n = (3a)^{3/4}/b$, at time $t = t_f = 3$ fm/c. (a) displays the beam energy dependence of a, b, and $\varepsilon^{3/4}/n$, and (b) exhibits the temperature dependence. The shaded areas indicate the range of a, b, and $\varepsilon^{3/4}/n$ for the case of a perfect gas of noninteracting massless quarks and gluons with $n_f = 2-4$ quark flavors and the same energy and particle densities as the real system.

constant. As a consequence $\varepsilon^{3/4}/n$ rises very slowly. The shaded areas indicate the range of a, b, and $\varepsilon^{3/4}/n$ if the partons would be a perfect gas of noninteracting massless quarks and gluons with $n_f = 2-4$ quark flavors, according to Eqs. (12) and (13), and the same energy and particle densities as the real system. In Fig. 13(b) the temperature dependence of a, b, and $\varepsilon^{3/4}/n$ is exhibited. The variation of a with increasing temperature is small and b is practically constant, which in view of Fig. 13(a) is not surprising, since the temperature itself increases only logarithmically with the beam energy. The shaded areas refer again to the corresponding behavior of an ideal parton gas.

From these considerations it is evident that at t_f =3 fm/c, measured in the center-of-mass frame, the partons in the central region of the nuclear collisions indeed establish an equilibrated state that closely resembles a dense and hot gas of quarks and gluons. Therefore one may assign this point of time to the initial time t_i^h for a subsequent hydrodynamical expansion for the quark-gluon plasma and introduce in analogy with Eq. (11) an effective equation of state interrelating pressure p and temperature T, together with the associated magnitude of the initial temperature at time t_i^h. Using Eqs. (12) and (41), the equation of state may be represented in the form

$$p(T) = \frac{\varepsilon}{3}\left(1+\frac{T}{a(T)}\frac{\partial a(T)}{\partial T}\right)^{-1} \simeq a(T)\,T^4 \quad , \qquad (44)$$

where the last equality is justified, because, as is obvious from Fig. 13(b), $\partial a(T)/\partial T \ll 1$. The temperature T and the function $a(T)$ refer here to the initial time for fluid dynamics, $t_i^h \equiv t_f$ =3 fm/c after the first instant of collision, which corresponds according to Eq. (39) to a proper time τ_i^h after the maximum nuclear overlap at $z = 0$ fm:

$$T(\tau_i^h, w) = 86.2\,\text{MeV}\ w^{-0.09}\ \ln(w),$$
$$a(\tau_i^h, w) = 4.95 + 0.3\left[\ln\left(\frac{w}{200}\right)\right]^{0.8} \quad , \qquad (45)$$

where

$$\tau_i^h = 2--2.6\ \text{fm}/c \quad \text{for } \sqrt{s}/A = 200--6300\ \text{GeV}, \qquad (46)$$

$$w = \frac{\sqrt{s}}{A\text{GeV}} \quad .$$

The initial conditions for fluid dynamics at the proper time τ_i^h can be expressed in terms of the associated energy density, particle density, respectively, entropy density, which may be parametrized as

$$\varepsilon(\tau_i^h, w) = 2.3\ \text{GeV fm}^{-3}\ w^{+0.05}\ \ln(w),$$
$$n(\tau_i^h, w) = 4.0\,\text{fm}^{-3}\ w^{-0.025}\ \ln(w), \qquad (47)$$
$$s(\tau_i^h, w) = 12.0\,\text{fm}^{-3}\ w^{+0.015}\ \ln(w) \quad .$$

These estimates are valid at least within a volume of 2 fm in longitudinal extension and 4 fm in transverse direction around the center of mass, i.e., a volume of about 100 fm^3. The equation of state and the initial conditions are therefore solely determined by the beam energy $\sqrt{s}$.

It is important to realize that the physical content of Eqs. (45) and (47) is, so to say, the condensed history of the early space-time evolution of the partons, as they approach an equilibrated state. In other words, the dynamics of the partons in phase space during the preequilibrium stage fixes the initial conditions for the further space-time development.

F. Multiplicities of pions from quark-gluon plasmas

Finally let me return to the question of measuring the amount of entropy produced during the early stage of a nuclear collision up to the formation of a quark-gluon plasma. As pointed out in Sec. II A, the entropy production vanishes in space-time when the system reaches a steady state of equilibrium. Furthermore, since the entropy is a constant of motion, once it has reached its final value, it is conserved throughout the subsequent expansion. Therefore the amount of entropy created in the central region allows for a direct estimate of the central multiplicity of final pions. This is the idea behind Eq. (21) which relates the entropy per unit rapidity dS/dy around $y = 0$ to the pion multiplicity $dN^{(\pi)}/dy$ at zero impact parameter. The possibility of additionally produced entropy during the hadronization process will not be considered here.

In the model calculations dS/dy is obtained from the computed rapidity distribution of secondary partons $dN^{(qg)}/dy$ via

$$\frac{dS}{dy} = \left(\frac{S}{N^{(qg)}}\right)\left(\frac{dN^{(qg)}}{dy}\right)_{b=0} \quad , \qquad (48)$$

where the entropy per parton $S/N^{(qg)}$ is given by the final equilibrium values at t =3 fm/c, $S/N^{(qg)} = 3.87-4.29$ for $\sqrt{s} = 200A$–$6300A$ GeV [Fig. 10(a)]. Inserting the computed dS/dy into formula (21),

$$\left(\frac{dN^{(\pi)}}{dy}\right)_{b=0} \simeq (0.19 \pm 0.06)\,\frac{dS}{dy} \quad , \qquad (21)$$

therefore gives an estimate for the central multiplicity of pions per unit rapidity, resulting from the quark-gluon plasma.

As shown in Fig. 14, the pion multiplicities in the central rapidity region around $y = 0$ predicted by this formula would be huge, because of the enormous amount of produced entropy: between $dN^{(\pi)}/dy = 1935 \pm 550$ ($\sqrt{s} = 200A$ GeV) and $dN^{(\pi)}/dy = 3430 \pm 980$ ($\sqrt{s} = 6300A$ GeV), increasing logarithmically with the beam energy. Even if these numbers are overestimated by a factor of 2, or so, such large pion production rates still would clearly reflect the tremendous entropy content of quark-gluon plasmas formed during the very early stage of the nuclear collisions. This is of particular value, since the total conserved entropy can be measured independent of the details of the equation of state and the further space-time evolution through the final pion spectra.

For comparison, also plotted in Fig. 14 is the more

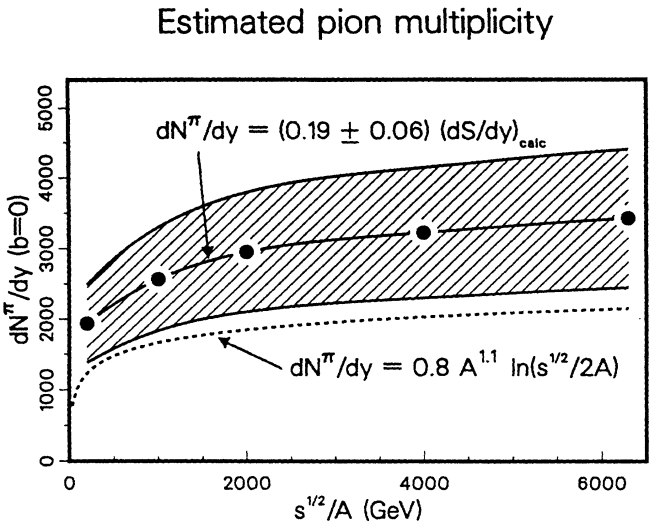

FIG. 14. The pion multiplicities in the central rapidity region around $y = 0$ estimated from the amount of total entropy in the central unit of rapidity, dS/dy, produced by the secondary partons during Au + Au collisions with $\sqrt{s} = 200A$–$6300A$ GeV. The points result from the computed values of dS/dy for the beam energies $\sqrt{s} = 200A$–$6300A$ GeV. Note that the predictions are based on the estimated ratio $r = 0.7 \pm 0.2$ of entropy densities between pion gas and quark-gluon plasma, which results in relatively large uncertainties as indicated by the shaded strip between the full curves. For comparison, the dotted curve corresponds to a more moderate empirical estimate for the multiplicity of pions obtained by extrapolation from pp and pA data.

moderate empirical estimate [38] for the multiplicity of pions around $y = 0$,

$$\left(\frac{dN^{(\pi)}}{dy}\right)_{b=0} = 0.8\, A^{\alpha}\, \ln\left(\frac{\sqrt{s}}{2A}\right) , \qquad (49)$$

obtained by extrapolation from pp and pA data, with $\alpha = 1.1$.

V. SUMMARY AND CONCLUSIONS

In this work I presented results of a complete phase-space analysis, obtained on the basis of the parton cascade model of Refs. [27,28]. The space-time development of central Au + Au collisions with $\sqrt{s} = 200A$–$6300A$ GeV during the first 3 fm/c was examined in terms of the evolution of energy, particle, and entropy densities of the secondary partons in the central collision region, defined as a cylindrical volume of 2 fm in length and a radius $R_{\rm Au}$ =6.7 fm centered at the nuclear center of mass. The thermodynamics of the preequilibrium stage and the process of parton thermalization was analyzed in both the center-of-mass time t at $z = 0$ fm and the proper time $\tau = \sqrt{(t - t_0)^2 - z^2}$, where $t_0 \equiv t_0(\sqrt{s})$ is the point of maximum nuclear overlap and z is the longitudinal distance from the center of mass (the collision point).

The results may be summarized as follows.

(i) By a time t_f =3 fm/c after the first instant of a central nuclear collision, very hot and dense plasmas of deconfined quarks and gluons with an effective number of quark flavors n_f =3–4 have been formed in the central region. The equilibrated quark-gluon matter extends over a volume of at least 100 fm^3. An extracted equation of state of the form $p(T) = a(T)T^4$ [see (vii) below] where p and T are the pressure and the temperature of the matter, describes the state of the plasmas in a way that closely resembles an ideal gas of partons.

(ii) During the first 3 fm/c the system of partons expands exclusively in longitudinal direction along the z axis. All volume elements expand approximately linearly with time and move in straight lines from the collision point at $z = 0$ fm with flow velocities that increase from the slowest expansion in the center of mass at $z = 0$ fm up to the speed of light in the fragmentation region of the receding beam fronts.

(iii) The maximum energy density is achieved between 1 fm/c and 0.4 fm/c, depending on the beam energy, and grows roughly linear with $\sqrt{s}$. The maximum particle density and entropy density show a moderate, aproximately logarithmic, increase.

(iv) The energy density ε, particle density n, and entropy density s reach spatially constant values around t_f =3 fm/c in the central collision region within about a volume of 2 fm in longitudinal extent and 4 fm radius in transverse extent. The magnitudes of ε, n, and s increase $\sim \ln(\sqrt{s}/A)$ with ε =15–31 GeV fm^{-3}, n =17.5–28 fm^{-3}, and s =67.5–120 fm^{-3} for $\sqrt{s} = 200A$–$6300A$ GeV.

(v) The decrease with proper time τ of ε, n, and s from their maximum values is beam energy dependent. For the various beam energies $\sqrt{s} = 200A$–$6300A$ GeV, the energy densities drop as $\varepsilon \sim \tau^{-\alpha}$, $\alpha \simeq 0.85$–1.1, the particle densities as $n \sim \tau^{-\beta}$, $\beta \simeq 0.6$–0.7, and the entropy densities as $s \sim \tau^{-\gamma}$, $\gamma \simeq 0.55$–0.65.

(vi) The temperatures associated with the time evolution of the densities ε, n, and s decrease as $T \simeq \tau^{-1/3}$. This proper time dependence is almost independent of the beam energy. The final temperatures at t_f =3 fm/c are in the range T =297–343 MeV for $\sqrt{s} = 200A$ GeV–$6300A$ GeV and show an approximate logarithmic increase $\sim \ln(\sqrt{s}/A)$.

(vii) The equation of state that determines the further evolution of the produced plasmas after $t_f = 3$ fm/c may be stated in the form $p(T) = a(T)\,T^4$ with initial temperature $T(\tau_i^h) = T(t_f)$, where $\tau_i^h = \sqrt{(t_f - t_0)^2 - z^2}$ is the initial proper time for the hydrodynamic expansion. This equation of state can be parametrized in terms of $w = \sqrt{s}/A$ GeV through $T(w) = 86.2$ MeV $w^{-0.09}$ $\ln(w)$ and $a(w) = 4.95 + 0.3\,[\ln(w/200)]^{0.8}$. It is the result of the space-time evolution of the partons during the preequilibrium stage of the collisions and implicitly takes into account the interactions among the partons, the time variation of the quark-gluon admixtures, and the effects associated with finite quark masses and nonvanishing central baryon density.

(viii) The total entropy per unit rapidity produced by the partons is related to the final pion multiplicity, $dN^{(\pi)}/dy \sim dS/dy$, which results in the prediction

of huge central pion multiplicities between $dN^{(\pi)}/dy = 1935 \pm 550$ ($\sqrt{s} = 200A$ GeV) and $dN^{(\pi)}/dy = 3430 \pm 980$ ($\sqrt{s} = 6300A$ GeV).

I have not addressed questions of experimental observables and signatures other than the final pion multiplicity associated with the entropy produced during the collisions. I do not intend to append here an *ad hoc* discussion of widely studied presumable quark-gluon plasma signatures [3–18]. However, I emphasize the important point that the particle production rates for direct photons, dileptons, strangeness, and charm essentially involve the knowledge of the amount of entropy produced. This quantity has generally been guessed in the past, thereby being a major source of uncertainty in estimates. Having in this work rigorously computed the entropy produced in ultrarelativistic nuclear collisions over a wide range of beam energies, it is appealing to reconsider the questions of characteristic particle production with these values as input.

It should be clear that the results presented here have been obtained within the specific framework of the parton cascade model. The reliability of this model essentially rests on the assumption that the nuclear dynamics during the first few fm/c, from the first instant of collision to the formation of an equilibrated quark-gluon plasma, is predominantly governed by independent parton-parton collisions plus associated parton emissions and absorption processes. If this assumption is correct, then the analysis presented in this paper is probably the most appropriate description of the early space-time evolution of ultrarelativistic nuclear collisions to date and the results should definitely have predictive power.

ACKNOWLEDGMENTS

Special thanks go to J. Kapusta for the stimulating discussions and his critical comments concerning this work. The numerical computations were mainly performed on the two Cray computers of the Minnesota Supercomputer Institute, which provided a generous amount of computer time. Additional calculations were done on a Silicon Graphics computer at Duke University, an opportunity for which I kindly thank B. Müller. This work was supported by the U.S. Department of Energy under Contract No. DOE/DE-FG02-87ER-40328.

[1] For an overview, see *Quark Matter '91*, Proceedings of the Ninth International Conference on Ultrarelativistic Nucleus-Nucleus Collisions, Gatlinburg, Tennessee, 1991, edited by T. C. Awes *et al.* [Nucl. Phys. **A544**, 1c (1992)]; *Quark Matter '90*, Proceedings of the Eighth International Conference on Ultrarelativistic Nucleus-Nucleus Collisions, Menton, France, 1990, edited by J. P. Blaizot *et al.* [Nucl. Phys. **A525**, 1c (1991)].

[2] *Quark Gluon Plasma*, edited by R. C. Hwa (World Scientific, Singapore 1990).

[3] *Quark Gluon Plasma Signatures*, Proceedings of the International Workshop, Strasbourg, France, 1991, edited by V. Bernard *et al.* (Editions Frontieres, Gif-sur-Yvette, France, 1991).

[4] E. V. Shuryak, Phys. Lett. **78B**, 150 (1978); Yad. Fiz. **28**, 796 (1978) [Sov. J. Nucl. Phys. **28**, 408 (1978)].

[5] K. Kajantie and H. Miettinen, Z. Phys. C **9**, 341 (1981).

[6] F. Halzen and H. C. Liu, Phys. Rev. D **25**, 1842 (1982).

[7] G. Staadt, W. Greiner, and J. Rafelski, Phys. Rev. D **33**, 66 (1986).

[8] D. K. Srivastava, B. Sinha, M. Gyulassy, and X.-N. Wang, Phys. Lett. B **276**, 285 (1986).

[9] J. Kapusta, P. Lichard, and D. Seibert, Phys. Rev. D **44**, 2774 (1991).

[10] L. D. McLerran and T. Toimela, Phys. Rev. D **31**, 545 (1985).

[11] R. C. Hwa and K. Kajantie, Phys. Rev. D **32**, 1109 (1985).

[12] K. Kajantie, M. Kataja, L. D. McLerran, and P. V. Ruuskanen, Phys. Rev. D **34**, 811 (1986).

[13] J. Kapusta, L. D. McLerran, and D. K. Srivastava, Phys. Lett. B **283**, 145 (1992).

[14] P. Koch, B. Müller, and J. Rafelski, Phys. Rep. **142**, 167 (1986).

[15] J. Kapusta and A. Mekjian, Phys. Rev. D **33**, 1304 (1986).

[16] T. Matsui, B. Svetitsky, and L. D. McLerran, Phys. Rev. D **34**, 783 (1986); **34**, 2047 (1986).

[17] A. Shor, Phys. Lett. B **215**, 375 (1988); **233**, 231 (1989).

[18] E. Shuryak, Phys. Rev. Lett. **68**, 3270 (1992).

[19] B. Müller and X.-N. Wang, Phys. Rev. Lett. **68**, 2437 (1992).

[20] L. D. Landau, Izv. Akad. Naul. SSSR, Ser. Fiz. **17**, 51 (1953).

[21] J. D. Bjorken, Phys. Rev. D **27**, 140 (1983).

[22] M. Gyulassy and T. Matsui, Phys. Rev. D **29**, 419 (1984).

[23] K. Kajantie, R. Raitio, and P. V. Ruuskanen, Nucl. Phys. **B222**, 152 (1983).

[24] G. Baym, B. L. Fryman, J.-P. Blaizot, M. Soyeur, and W. Czyz, Nucl. Phys. **A407**, 541 (1983).

[25] H. Gersdorff, L. D. McLerran, M. Kataja, and P. V. Ruuskanen, Phys. Rev. D **34**, 794 (1986).

[26] N. S. Amelin, E. F. Straubo, L. P. Csernai, V. D. Toneev, K. K. Gudima, and D. D. Strottman, Phys. Rev. Lett. **67**, 1523 (1991).

[27] K. Geiger and B. Müller, Nucl. Phys. **B369**, 600 (1991).

[28] K. Geiger, preceding paper, Phys. Rev. D **46**, 4965 (1992).

[29] S. de Groot, W. A. van Leuwen, and C. G. van Weert, *Relativistic Kinetic Theory* (North-Holland, Amsterdam, 1980).

[30] J. Kapusta, Nucl. Phys. **B148**, 461 (1979).

[31] E. V. Shuryak, Phys. Rep. **115**, 151 (1984).

[32] L. P. Csernai and J. Kapusta, Phys. Rev. Lett. **69**, 737 (1992).

[33] G. Bertsch and J. Cugnon, Phys. Rev. C **24**, 2514 (1981).

[34] J. Randrup, Nucl. Phys. **A314**, 429 (1979).

[35] Since with increasing beam energy the projectiles become more Lorentz contracted along the beam direction ($\gamma \simeq 107$–3354 for $\sqrt{s}/A = 200$–6300 GeV), the time that it takes from the first contact at $t = 0$ fm/c until the nuclei reach their maximum overlap is energy dependent

it takes from the first contact at $t = 0$ fm/c until the nuclei reach their maximum overlap is energy dependent with values $t_0(\sqrt{s})$=1, 0.75, 0.55, 0.45, 0.40 fm/c for $\sqrt{s}/A$=200, 1000, 2000, 4000, 6300 GeV. These values result from the distribution of partons in the incoming nuclei: Whereas the valence quarks are contracted to a thin disk of longitudinal extension $\Delta z_v = 2R_A/\cosh Y$ ($Y \simeq \ln 2\gamma$ is the rapidity of the nuclei), the majority of gluons and sea quarks have rapidities $y \ll Y$ and are longitudinally smeared out over $\Delta z_{g,s} \sim 1/p_z \simeq 1/p_\perp \sinh y$, where $\langle p_\perp \rangle \simeq 0.38$ GeV is the average transverse momentum of the primordial partons [28]. With increasing beam energy the average rapidity of the soft partons grows too, with the result that they occupy a Lorentz-contracted volume with a longitudinal extension that effectively decreases as $\Delta z_{g,s} \propto 2R_A/\ln\gamma$.

[36] Note that in Fig. 7 the exact points of the maximum energy, particle, and entropy densities lie somewhere between the data points. Because of the complexity of the computations the number of time steps selected for the phase-space analysis during the collisions was limited to ten, so that a finer resolution of the space-time development was impractical.

[37] This statement deserves some comment. Aside from the fact that with increasing beam energy the point of maximum overlap of the projectiles is shifted towards earlier times (see [35]), the dynamics of the partons changes in the following manner: With growing beam energy not only the initial number of sea quarks and gluons surrounding the valence quarks [27,28] becomes larger, but also the average initial parton momentum increases. This results in more numerous and, on the average, more energetic parton collisions that in turn give rise to a faster production of additional gluons and quark-antiquark pairs. The multiplicity of the newly produced particles also increases as the initiating parton collisions become harder. Upon their initial contact, the nuclei become increasingly black until further particle production will be suppressed due to the superdense phase-space population and parton recombination processes begin work in the opposite direction [27]. All together the effect is a more and more violent "initial clash." In accordance with that, the energy-momentum brought into the nuclear collision is distributed and harnessed quicker. This is reflected by the shorter relaxation times for larger beam energies.

[38] H. Satz, talk given at the CERN Heavy Ion Workshop, Geneva, Switzerland, 1991; in *Quark Matter '91* [1].

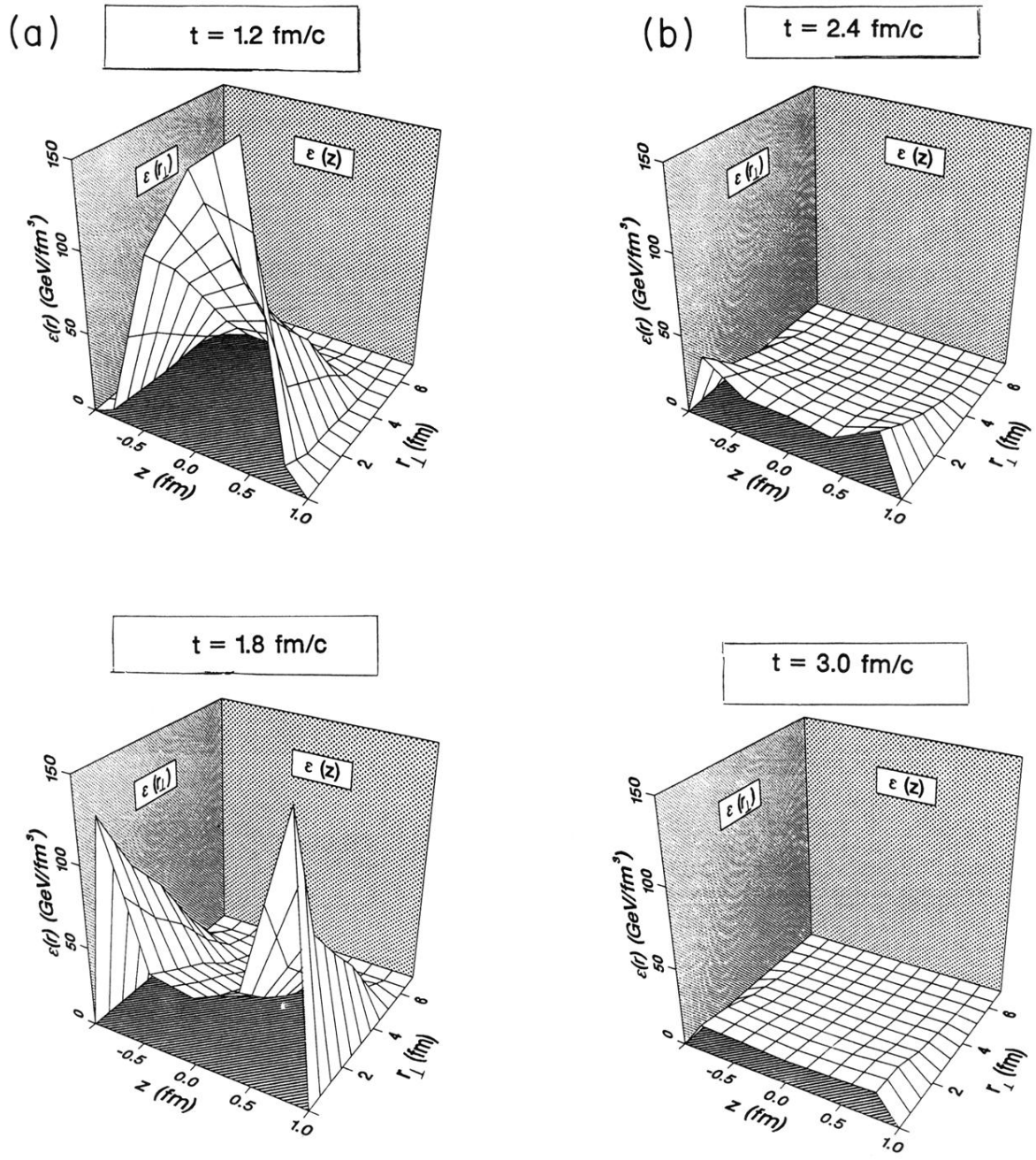

FIG. 6. Time development of the energy density profile in the central region of a Au + Au collision with $\sqrt{s} = 200A$ GeV. The snapshots exhibit the space-time evolution of the energy density of the secondary partons in four characteristic profiles between t =1.4 fm/c ($\simeq$ 0.4 fm/c after the maximum density was achieved) and t =3 fm/c. Note that in transverse direction the density profiles are weighted by $r_\perp^{-1}$, i.e., $\varepsilon(r_\perp) = dE/r_\perp dr_\perp$.